

# Weak interaction corrections to hadronic top quark pair production

Werner Bernreuther <sup>a,\*</sup>, Michael Fűcker <sup>a,†</sup>, Zong-Guo Si <sup>b,‡</sup>

<sup>a</sup>Institut für Theoretische Physik, RWTH Aachen, 52056 Aachen, Germany

<sup>b</sup>Department of Physics, Shandong University, Jinan, Shandong 250100, China

## Abstract

In this paper we determine the weak-interaction corrections of order  $\alpha_s^2\alpha$  to hadronic top-quark pair production. First we compute the one-loop weak corrections to  $t\bar{t}$  production due to gluon fusion and the order  $\alpha_s^2\alpha$  corrections to  $t\bar{t}$  production due to (anti)quark gluon scattering in the Standard Model. With our previous result [21] this yields the complete corrections of order  $\alpha_s^2\alpha$  to  $gg$ ,  $q\bar{q}$ ,  $qg$ , and  $\bar{q}g$  induced hadronic  $t\bar{t}$  production with  $t$  and  $\bar{t}$  polarizations and spin-correlations fully taken into account. For the Tevatron and the LHC we determine the weak contributions to the transverse top-momentum and to the  $t\bar{t}$  invariant mass distributions. At the LHC these corrections can be of the order of 10 percent compared with the leading-order results, for large  $p_T$  and  $M_{t\bar{t}}$ , respectively. Apart from parity-even  $t\bar{t}$  spin correlations we analyze also parity-violating double and single spin asymmetries, and show how they are related if CP invariance holds. For  $t$  (and  $\bar{t}$ ) quarks which decay semileptonically, we compute a resulting charged-lepton forward-backward asymmetry  $A_{PV}$  with respect to the  $t$  ( $\bar{t}$ ) direction, which is of the order of one percent at the LHC for suitable invariant-mass cuts.

PACS number(s): 12.15.Lk, 12.38.Bx, 13.88.+e, 14.65.Ha

Keywords: hadron collider physics, top quarks, QCD and electroweak corrections, spin effects, parity violation, CP violation

---

\*Email: breuther@physik.rwth-aachen.de

†Email: fuecker@physik.rwth-aachen.de

‡Email: zgisi@sdu.edu.cn

# 1. Introduction

Even after a decade of experimental research at the Tevatron, the top quark is still a relatively unexplored particle as compared to the other quarks and leptons. The situation will change once the LHC will operate with planned luminosity, as it is expected that the large event rates will allow for precise investigations of these quarks. Full exploration of the data requires also precise theoretical predictions for top quark production and decay, especially within the Standard Model (SM).

As far as hadronic top quark pair production is concerned, predictions for unpolarized  $t\bar{t}$  production have long been known at next-to-leading order (NLO) QCD [1,2,3,4,5,6], and these NLO results were refined by resummation of soft gluon and threshold logarithms [7, 8, 9, 10, 11]. Moreover,  $t\bar{t}$  production and decay including the full spin degrees of freedom of the intermediate  $t$  and  $\bar{t}$  resonances were determined to NLO QCD some time ago [12, 13, 14, 15]. Top quark spin effects can be reliably predicted in view of the extremely short lifetime of these quarks, that is, the short-distance nature of their interactions, and are expected to play an important role in refined data analyses.

A complete NLO analysis of  $t\bar{t}$  production within the SM should include also the electroweak interactions. While they are not relevant for the production cross section  $\sigma_{t\bar{t}}$  at the Tevatron and at the LHC (see Section 3 below), they may be important for distributions at large transverse top momentum or large  $t\bar{t}$  invariant mass due to large Sudakov logarithms<sup>1</sup>. Moreover, the weak interactions induce small parity-violating effects, and for full exploration and interpretation of future data it is important to obtain definite SM predictions also for these effects.

Weak interaction corrections to hadronic  $t\bar{t}$  production were studied so far in a number of papers. The order  $\alpha_s^2\alpha$  weak-QCD corrections to  $q\bar{q} \rightarrow t\bar{t}$  and  $gg \rightarrow t\bar{t}$  of order  $\alpha_s^2\alpha$  were analyzed in [19] (see also [20]). Full determinations of these corrections to  $q\bar{q} \rightarrow t\bar{t}(g)$ , including the infrared-divergent box contributions and the corresponding real gluon radiation were made in [21, 22]. Recently the order  $\alpha_s^2\alpha$  corrections to  $gg \rightarrow t\bar{t}$  including the quark triangle diagrams  $gg \rightarrow Z \rightarrow t\bar{t}$  were investigated in [23]. (Cf. [24, 25] and references therein for weak corrections to other four-parton processes.) In [26, 20, 27, 21, 28] parity violation in  $t\bar{t}$  production was analyzed within the SM. Investigations of non-SM effects include refs. [30, 29, 27, 31].

In this paper we present results based on our determination of the complete weak interaction corrections of order  $\alpha_s^2\alpha$  to  $gg \rightarrow t\bar{t}$ , to  $q\bar{q} \rightarrow t\bar{t}(g)$ , and for completeness also for  $gq(\bar{q}) \rightarrow t\bar{t}q(\bar{q})$ , with  $t$  and  $\bar{t}$  polarizations and spin-correlations fully taken into account. For  $t\bar{t}$  production at the Tevatron and the LHC we determine the weak contributions to a number of top spin-(in)dependent distributions. As far as parity-violating effects are concerned, we derive, for arbitrary  $t$  and  $\bar{t}$  spin bases, a relation between a parity-violating double spin-asymmetry and corresponding single spin asymmetries. For the helicity basis this implies that the parity-violating double spin-asymmetry is equal to the corresponding single spin asymmetry if CP invariance holds in hadronic  $t\bar{t}$  production. Taking into account all contributions to order  $\alpha_s^2\alpha$  we compute this spin asymmetry for the Tevatron and the LHC as a function of the  $t\bar{t}$  invariant mass. This observable may serve as a useful tool in exploring the dynamics of hadronic  $t\bar{t}$  production. For some of the observables considered in this paper the weak corrections were analyzed before in the literature; however, these analyses did not take into account the complete order  $\alpha_s^2\alpha$  corrections. We compare with these results where possible.

The paper is organized as follows. In Section 2 we present our results for the order  $\alpha_s^2\alpha$  weak corrections

---

<sup>1</sup>See, e.g., [16, 17, 18] for reviews and references concerning electroweak Sudakov logarithms.

to  $gg \rightarrow t\bar{t}$ , both for the partonic cross section and for  $t$ ,  $\bar{t}$  polarization and  $t\bar{t}$  spin-correlation observables. We discuss the size of the weak corrections versus leading order (LO) QCD results, and make an explicit comparison with NLO QCD in the case of the partonic cross section. For the reactions  $gq(\bar{q}) \rightarrow t\bar{t}q(\bar{q})$  we calculate the order  $\alpha_s^2\alpha$  weak corrections to the partonic cross sections and to  $t$  and  $\bar{t}$  spin observables. Then we derive, for the partonic collisions that initiate  $t\bar{t}$  production, several relations involving top-spin observables. In particular, we show that the parity-violating single and double spin-asymmetries are not independent observables. In this and in the next section we comment also briefly on a CP-violating asymmetry. In Section 3 we give our results at the level of hadronic collisions. We determine the order  $\alpha_s^2\alpha$  weak corrections to the  $t\bar{t}$  cross section at the Tevatron and at the LHC. We compute the weak interaction corrections to the transverse top-momentum and the  $t\bar{t}$  invariant mass distribution, and to two parity-invariant double spin asymmetries. Moreover, we determine the above-mentioned parity-violating double spin asymmetry in the helicity basis, which is equal to the corresponding single  $t$  spin asymmetry, as a function of  $M_{t\bar{t}}$  and determine the resulting charged-lepton forward-backward asymmetry for semileptonic  $t$  quark decays. We conclude in Section 4.

## 2. Parton level results

At the Tevatron and at the LHC top quark pairs are produced predominantly by the strong interactions. Theoretical predictions for the subprocesses  $i \rightarrow t\bar{t} + X$ , ( $i = q\bar{q}, gg, gq, g\bar{q}$ ) are known to order  $\alpha_s^3$ . The leading corrections to these parton processes involving electroweak interactions are, for  $i = q\bar{q}$ , the order  $\alpha^2$  Born contributions (from  $q\bar{q} \rightarrow \gamma, Z \rightarrow t\bar{t}$ ) and, for  $i = q\bar{q}$  and  $gg$ , the mixed QCD electroweak corrections of order  $\alpha_s^2\alpha$ . Due to color conservation there are no corrections of order  $\alpha_s\alpha$ .

In [21] we have determined the weak corrections of order  $\alpha_s^2\alpha$  for  $q\bar{q}$  initiated top-pair production, which involve the reactions  $q\bar{q} \rightarrow t\bar{t}$  and  $q\bar{q} \rightarrow t\bar{t}g$ ; see also [22]. Here we consider gluon-gluon fusion,

$$g(p_1) + g(p_2) \rightarrow t(k_1, s_t) + \bar{t}(k_2, s_{\bar{t}}), \quad (2.1)$$

and we present in this section our results for the weak interaction effects on the cross section and on several single and double spin observables of this parton reaction. In (2.1) the parton momenta are denoted by  $p_1$ ,  $p_2$ ,  $k_1$ , and  $k_2$ , and the vectors  $s_t$ ,  $s_{\bar{t}}$ , with  $s_t^2 = s_{\bar{t}}^2 = -1$  and  $k_1 \cdot s_t = k_2 \cdot s_{\bar{t}} = 0$  describe the spin of the top and antitop quark. The leading correction involving electroweak interactions<sup>2</sup> to the differential cross section of (2.1) is of the form

$$\alpha_s^2\alpha \delta\mathcal{M}_W(p, k, s_t, s_{\bar{t}}). \quad (2.2)$$

We are interested here only in purely weak, in particular in parity-violating effects. Therefore we take into account only the mixed QCD and weak contributions to  $\delta\mathcal{M}_W$  in the following. The photonic contributions form a gauge invariant set and can be straightforwardly obtained separately. The contributions to  $\delta\mathcal{M}_W$  are the  $gg \rightarrow t\bar{t}$  QCD Born diagrams interfering with the 1-loop diagrams involving the weak gauge boson, Goldstone boson (we work in the 't Hooft Feynman gauge), and Higgs boson exchanges which yield top quark self-energy, vertex, box-diagram, and, via quark triangle diagrams, s-channel  $Z$ –

---

<sup>2</sup>Although we consider in this paper purely weak corrections, we parameterize our results for convenience in terms of the QED coupling  $\alpha = \alpha_W \sin^2\theta_W$ .

and Higgs-boson contributions [19]. The diagrams are shown in Fig. 1a. The ultraviolet divergences in the self-energy and vertex corrections are removed using the on-shell scheme [19] for defining the wave function renormalizations of  $t_L$  and  $t_R$  and the top quark mass  $m_t$ . All the 1-loop purely weak contributions to (2.1) are infrared-finite.

We take into account also the 1-loop amplitudes  $gg \rightarrow Z, \chi^0 \rightarrow t\bar{t}$ , where  $Z$  denotes an off-shell  $Z$  boson and  $\chi^0$  is the corresponding neutral Goldstone boson. The  $gg \rightarrow Z$  vertex is induced by the flavor non-singlet neutral axial vector current  $J_{5\mu}^{NS} = \sum_{i=1}^3 \bar{\psi}_i \gamma_\mu \gamma_5 \tau_3 \psi_i$ , where  $\psi_i = (u, d)_i$  is the  $i$ -th generation quark isodoublet and  $\tau_3$  is the 3rd Pauli matrix. Because of the large  $t, b$  quark-mass splitting, only the contribution of the third quark generation matters. In this paper we take all quarks but the top quark to be massless. The  $gg \rightarrow \chi^0$  vertex is generated by the corresponding pseudoscalar current  $J_5^{NS}$ . The contribution of  $gg \rightarrow Z, \chi^0 \rightarrow t\bar{t}$  to  $\delta\mathcal{M}_W$  – which we shall denote by “non-singlet neutral current contribution” in the following – was apparently not considered in [19], but was taken into account in the recent paper [23].

We have determined (2.2) analytically for arbitrary  $t$  and  $\bar{t}$  spin states. From this expression one can extract the weak interaction corrections to the  $gg \rightarrow t\bar{t}$  spin density matrix. This matrix, when combined with the decay density matrices describing semi- and non-leptonic  $t$  and  $\bar{t}$  decay yields predictions at the level of the  $t$  and/or  $\bar{t}$  decay products of the order  $\alpha_s^2 \alpha$  weak interaction effects in top-pair production. Likewise one may proceed with the weak corrections to  $q\bar{q} \rightarrow t\bar{t}(g)$  [21].

For the sake of brevity we do not give here the expression for  $\delta\mathcal{M}_W(p, k, s_t, s_{\bar{t}})$ , but present results for the weak corrections to the partonic cross section and to several single and double spin asymmetries, which we believe are of interest to phenomenology. The inclusive, spin-summed cross section for (2.1) may be written, to NLO in the SM gauge couplings, in the form

$$\sigma_{gg} = \sigma_{gg}^{(0)} + \delta\sigma_{gg}^{(1)} + \delta\sigma_{gg}^W, \quad (2.3)$$

where the first and second term are the LO (order  $\alpha_s^2$ ) and NLO (order  $\alpha_s^3$ ) QCD contributions [1, 2, 3, 4, 13], and the third term denotes the weak corrections described above. We parameterize this term as follows:

$$\delta\sigma_{gg}^W(\hat{s}, m_t^2) = \frac{4\pi\alpha_s^2\alpha}{m_t^2} f_{gg}^{(1W)}(\eta), \quad (2.4)$$

where  $\eta = \hat{s}/4m_t^2 - 1$ , with  $\hat{s}$  being the gluon-gluon center-of-mass (c.m.) energy squared. We have numerically evaluated the scaling function  $f_{gg}^{(1W)}(\eta)$  – and those defined below – and parameterized them in terms of fits which allow for a quick use in applications. In the following we use  $m_Z = 91.188$  GeV,  $\sin^2\theta_W = 0.231$ , and  $m_t = 172.7$  GeV [32, 33]. As already mentioned, all quarks but the top quark are taken to be massless. Moreover, we use two values of the Higgs boson mass,  $m_H = 120$  GeV and  $m_H = 200$  GeV, which correspond approximately to the present experimental lower and upper bound on  $m_H$ . Moreover,  $\alpha_s(2m_t) = 0.1$  and  $\alpha(2m_t) = 1/126.3$  were chosen in the results given below. In the  $s$ -channel Higgs exchange diagram we take into account the finite width of the Higgs boson; however, for the chosen range of  $m_H$  this is numerically insignificant.

In Fig. 2 we have plotted the ratio

$$r_W^{(0)} = \frac{\delta\sigma_{gg}^W}{\sigma_{gg}^{(0)}} \quad (2.5)$$

as a function of  $\eta$  for the two Higgs masses given above. This figure shows that the non-singlet neutral current contribution is relevant, as compared to the other weak corrections, in the vicinity of the  $t\bar{t}$  threshold up to  $\eta \sim 1$ . The weak interaction corrections to  $\sigma_{gg}$  are essentially negative for all Higgs-boson masses above the present experimental lower bound – except for  $m_H \leq 120\text{GeV}$  very close to threshold. The weak corrections (2.4) to the cross section of the  $gg$  subprocess and  $r_W^{(0)}$  have recently been computed also by [34]. We have compared our results and find excellent numerical agreement. Moreover, we have evaluated our results for (2.4), excluding the non-singlet neutral current contribution, with the parameter values chosen in [19] and compared with the results given in Figs. 11 - 16 of that paper, with which we also agree.

From Fig. 2 one might conclude that for large  $\sqrt{\hat{s}}$  the weak corrections to  $\sigma_{gg}$  grow as compared with the QCD cross section. However, this is deceptive: the NLO QCD corrections must be taken into account for a realistic assessment of the high energy behavior. Real gluon radiation,  $gg \rightarrow t\bar{t}g$ , involves  $t$ - and  $u$ -channel gluon exchange diagrams, which are dominant at high energies, while such exchanges of massless spin-one particles are absent at lowest order QCD and for the weak corrections of order  $\alpha_s^2\alpha$ . This causes the NLO QCD corrections to  $\sigma_{gg}$  to approach a constant for large  $\hat{s}$  [1] while the Born cross section falls off. Thus the NLO QCD corrections to the  $gg$  initiated  $t\bar{t}$  production show a high-energy behaviour<sup>3</sup> which is strikingly different from the QCD corrections to  $q\bar{q}$  induced top-pair production, which fall off for large  $\sqrt{\hat{s}}$ . Moreover, we recall that the NLO QCD corrections to  $q\bar{q}$  and  $gg$  initiated cross sections are large in the vicinity of the  $t\bar{t}$  threshold due to the exchange of Coulomb gluons.

Fig. 3 exhibits the ratio

$$r_W^{(1)} = \frac{\delta\sigma_{gg}^W}{\sigma_{gg}^{(0)} + \delta\sigma_{gg}^{(1)}} \quad (2.6)$$

as a function of  $\eta$  for  $m_H = 120\text{ GeV}$  and three values of the renormalization scale  $\mu$ , which is put equal to the factorization scale. In this Figure the coupling  $\alpha_s(\mu)$  has been evaluated according to two-loop renormalization group evolution. Fig. 3 shows that the weak corrections to  $\sigma_{gg}$ , which are negative, do not exceed  $\sim 3\%$  in magnitude. The size and location of the maximum of  $|r_W^{(1)}|$  depends on the scale  $\mu$ . Eventually, the significance of the weak corrections must be investigated at the level of hadronic collisions.

For completeness we have determined the order  $\alpha_s^2\alpha$  corrections to the partonic cross sections also for the reactions  $gq(\bar{q}) \rightarrow t\bar{t}q(\bar{q})$ . These corrections arise from the interference of the QCD and the mixed electroweak-QCD diagrams shown in Fig. 1b. Notice that the diagram involving the three-gluon vertex does not interfere with the mixed diagrams due to color mismatch. Writing  $\sigma_{qg} = \sigma_{qg}^{(1)} + \delta\sigma_{qg}^W$ , where  $\sigma_{qg}^{(1)}$  is the order  $\alpha_s^3$  Born cross section, we parameterize  $\delta\sigma_{qg}^W$  in analogy to (2.4):

$$\delta\sigma_{qg}^W(\hat{s}, m_t^2) = \frac{4\pi\alpha_s^2\alpha}{m_t^2} f_{qg}^{(1W)}(\eta). \quad (2.7)$$

From crossing symmetry we have  $f_{\bar{q}g}^{(1W)}(\eta) = f_{qg}^{(1W)}(\eta)$ . The scaling function for u-type quarks,  $f_{qg}^{(1W)}(\eta)$  is shown in Fig. 4, upper frame. For d-type quarks  $f_{dg}^{(1W)}(\eta) = -f_{ug}^{(1W)}(\eta)$  holds. This is due to the fact that in the interference terms of the weak interaction diagrams, involving the  $\gamma t\bar{t}$  and  $Z t\bar{t}$  vertices, and the

---

<sup>3</sup>This applies also to  $gq(\bar{q})$  initiated  $t\bar{t}$  production [1].

QCD diagrams the terms that are generated by the vector currents vanish due to Furry's theorem, and  $f_{qg}^{(1W)}$  is proportional to  $a_q a_t$ , where  $a_q$  is the neutral-current axial-vector coupling. For the Tevatron and the LHC the corrections (2.7) are small as compared to  $\sigma_{qg}^{(1)}$ , which in turn makes only a small contribution to the  $t\bar{t}$  cross section, as compared with  $gg$  and  $q\bar{q}$  initiated production. For the hadronic cross section to be discussed in the next section, we will therefore take into account only these initial parton states.

Next we consider observables that involve the  $t$  and/or  $\bar{t}$  spin. Denoting the top spin operator by  $\mathbf{S}_t$  and its projection onto an arbitrary unit vector  $\hat{\mathbf{a}}$  by  $\mathbf{S}_t \cdot \hat{\mathbf{a}}$  we can express its unnormalized partonic expectation value, which we denote by double brackets, in terms of the difference between the ‘‘spin up’’ and ‘‘spin down’’ cross sections:

$$2\langle\langle\mathbf{S}_t \cdot \hat{\mathbf{a}}\rangle\rangle_i = \sigma_i(\uparrow) - \sigma_i(\downarrow), \quad (2.8)$$

where  $\langle\langle O \rangle\rangle_i \equiv \int d\sigma_i O$ . Here  $i$  denotes one of the partonic initial states that produce  $t\bar{t}$ , and the arrows refer to the projection of the top-quark spin onto  $\hat{\mathbf{a}}$ . An analogous formula holds for the antitop quark. It is these expressions that enter the corresponding predictions at the level of hadronic collisions.

There are two types of single spin asymmetries (2.8): parity-even, T-odd asymmetries<sup>4</sup>, where the spin projection is onto an axial vector, and parity-odd, T-even ones where  $\hat{\mathbf{a}}$  is a polar vector. The asymmetry associated with the projection of  $\mathbf{S}_t$  onto the normal of the  $q, t$  scattering plane belongs to the first class. It is induced by the parity-even absorptive part of  $\delta\mathcal{M}_W$ , but also by the absorptive part of the NLO QCD amplitude. The QCD-induced  $t$  and  $\bar{t}$  polarization normal to the scattering plane is of the order of a few percent [36, 37]. The weak contribution is even smaller; therefore we do not display it here.

The P-odd, T-even single spin asymmetries correspond to a polarization of the  $t$  (and  $\bar{t}$ ) quarks along a polar vector, in particular along a direction in the scattering plane. Needless to say, these asymmetries cannot be generated within QCD; the SM contribution results from the parity-violating part of  $\delta\mathcal{M}_W$ . Popular choices are top-spin projections onto the beam axis [15] and the off-diagonal axis  $\hat{\mathbf{d}}_{\text{off}}$  [38], which are relevant for the Tevatron, and onto the helicity axes, which are relevant for the LHC. These axes must be defined in a collinear safe reference frame, and a convenient one with this property is the  $t\bar{t}$  zero-momentum frame (ZMF) [15]. With respect to this frame we define

$$\hat{\mathbf{a}} = \hat{\mathbf{b}} = \hat{\mathbf{p}}, \quad (\text{beam basis}), \quad (2.9)$$

$$\hat{\mathbf{a}} = -\hat{\mathbf{b}} = \hat{\mathbf{k}}, \quad (\text{helicity basis}), \quad (2.10)$$

where  $\hat{\mathbf{k}}$  denotes the direction of flight of the top quark in the  $t\bar{t}$  ZMF and  $\hat{\mathbf{p}}$  is the direction of flight of one of the colliding hadrons in that frame. The direction of the hadron beam can be identified to a very good approximation with the direction of flight of one of the initial partons. The unit vector  $\hat{\mathbf{b}}$  serves as quantization axis for the  $\bar{t}$  quark spin. In fact, the beam and off-diagonal axes are useless here, as we have the result (which is exact for the  $gg \rightarrow t\bar{t}$  amplitude):

$$\langle\langle\mathbf{S}_t \cdot \hat{\mathbf{p}}\rangle\rangle_{gg} = \langle\langle\mathbf{S}_t \cdot \hat{\mathbf{d}}_{\text{off}}\rangle\rangle_{gg} = 0. \quad (2.11)$$

Eq. (2.11) follows from the properties of the coefficients of the  $gg \rightarrow t\bar{t}$  spin density matrix dictated by Bose symmetry of the initial  $gg$  state, which were derived in [41]. As to the helicity basis, the

---

<sup>4</sup>T-even/odd refers to the behavior with respect to a naive T transformation, i.e., reversal of momenta and spins.

unnormalized expectation value of  $\mathbf{S}_t \cdot \hat{\mathbf{k}}$  is again conveniently expressed by a scaling function:

$$\langle\langle 2\mathbf{S}_t \cdot \hat{\mathbf{k}} \rangle\rangle_{gg} = \frac{4\pi\alpha_s^2\alpha}{m_t^2} h_{gg}^{(1W, hel)}(\eta). \quad (2.12)$$

The scaling function  $h_{gg}^{(1W, hel)}$  is shown in Fig. 5. Notice that  $\langle\langle 2\mathbf{S}_t \cdot \hat{\mathbf{a}} \rangle\rangle$  does not depend on  $m_H$ , as the SM Higgs boson exchange is parity-conserving. While the non-singlet neutral current diagrams do contribute to  $\sigma_{gg}$  and to several spin-correlation observables, they have no effect on  $h_{gg}^{(1W, hel)}$ . This follows from the structure of the non-singlet neutral-current contribution to  $\delta\mathcal{M}_W$ .

We have computed the expectation value of this observable also for  $qg$  and  $\bar{q}g$  initiated  $t\bar{t}$  production. Using a parameterization analogous to (2.12),

$$\langle\langle 2\mathbf{S}_t \cdot \hat{\mathbf{k}} \rangle\rangle_j = \frac{4\pi\alpha_s^2\alpha}{m_t^2} h_j^{(1W, hel)}(\eta), \quad j = qg, \bar{q}g, \quad (2.13)$$

the scaling functions  $h_j^{(1W, hel)}$  are shown in Fig. 4, lower frame, for  $j = ug, \bar{u}g, dg, \text{ and } \bar{d}g$ . Notice that the expectation value of  $\mathbf{S}_t \cdot \hat{\mathbf{k}}$  is different for  $qg$  and  $\bar{q}g$  initiated reactions.

Next we analyze top-antitop spin correlations. The most interesting set of spin observables besides (2.8) seem to be, as far as SM weak interaction effects are concerned, parity-violating double spin asymmetries defined by the following difference of spin-dependent cross sections:

$$D_i(\uparrow\downarrow) \equiv \sigma_i(\uparrow\downarrow) - \sigma_i(\downarrow\uparrow), \quad i = q\bar{q}, gg, gq, g\bar{q}, \quad (2.14)$$

where the first (second) arrow on the right-hand side of (2.14) refers to the  $t$  ( $\bar{t}$ ) spin projection onto a polar vector  $\hat{\mathbf{a}}$  ( $\hat{\mathbf{b}}$ ). It is obvious that a nonzero  $D_i(\uparrow\downarrow)$  requires P-violating interactions; there are, as in the case of (2.12), no QCD and QED contributions to (2.14) to any order in the gauge couplings.

There is a useful relation between these P-violating double spin asymmetries and the single-spin observables discussed above. Using the consequences of rotational invariance for the  $i \rightarrow t\bar{t} + X$  spin density matrices [41], we obtain the following exact result:

$$2D_i(\uparrow\downarrow) = \langle\langle 2\mathbf{S}_t \cdot \hat{\mathbf{a}} - 2\mathbf{S}_{\bar{t}} \cdot \hat{\mathbf{b}} \rangle\rangle_i, \quad i = q\bar{q}, gg, gq, g\bar{q}. \quad (2.15)$$

That is, the asymmetries (2.14) are completely determined by the corresponding single  $t$  and  $\bar{t}$  spin observables.

For the LHC useful reference axes  $\hat{\mathbf{a}}, \hat{\mathbf{b}}$  are the helicity axes (2.10). In this case we use the notation  $D_i(\uparrow\downarrow) = D_{RL,i}$ , and (2.15) reads:

$$2D_{RL,i} = \langle\langle 2\mathbf{S}_t \cdot \hat{\mathbf{k}}_t - 2\mathbf{S}_{\bar{t}} \cdot \hat{\mathbf{k}}_{\bar{t}} \rangle\rangle_i = \langle\langle (2\mathbf{S}_t + 2\mathbf{S}_{\bar{t}}) \cdot \hat{\mathbf{k}} \rangle\rangle_i, \quad (2.16)$$

where  $\hat{\mathbf{k}}$  is the  $t$  direction in the  $t\bar{t}$  ZMF. If the interactions that affect  $i \rightarrow t\bar{t} + X$  are CP-invariant then

$$D_{RL,i} = \langle\langle 2\mathbf{S}_t \cdot \hat{\mathbf{k}}_t \rangle\rangle_i = -\langle\langle 2\mathbf{S}_{\bar{t}} \cdot \hat{\mathbf{k}}_{\bar{t}} \rangle\rangle_i, \quad i = q\bar{q}, gg, \quad (2.17)$$

must hold. Eq. (2.17) constitutes a CP-symmetry test in  $t\bar{t}$  production. In fact, SM CP violation, i.e., the Kobayashi-Maskawa phase leads to tiny CP-violating effects (which are induced beyond the 1-loop approximation) in flavor-diagonal reactions like those considered here. Thus an experimentally detectable

violation of Eq. (2.17) requires non-standard CP-violating interactions (see below).

Let us, for completeness, also discuss the expectation value of the single spin observable for the reactions  $qg, \bar{q}g \rightarrow t\bar{t}X$ . For CP invariant interactions we obtain:

$$\langle\langle 2\mathbf{S}_t \cdot \hat{\mathbf{k}}_t \rangle\rangle_{q(\mathbf{p}_1)g(\mathbf{p}_2)} = -\langle\langle 2\mathbf{S}_{\bar{t}} \cdot \hat{\mathbf{k}}_{\bar{t}} \rangle\rangle_{\bar{q}(-\mathbf{p}_1)g(-\mathbf{p}_2)} = -\langle\langle 2\mathbf{S}_{\bar{t}} \cdot \hat{\mathbf{k}}_{\bar{t}} \rangle\rangle_{\bar{q}(\mathbf{p}_1)g(\mathbf{p}_2)}, \quad (2.18)$$

and an analogous relation holds for  $\langle\langle 2\mathbf{S}_t \cdot \hat{\mathbf{k}}_t \rangle\rangle_{\bar{q}g}$ . The last equation in (2.18) follows from rotational invariance. These relations and (2.15) imply

$$D_{RL,qg} = D_{RL,\bar{q}g} = \langle\langle \mathbf{S}_t \cdot \hat{\mathbf{k}}_t \rangle\rangle_{qg} + \langle\langle \mathbf{S}_t \cdot \hat{\mathbf{k}}_t \rangle\rangle_{\bar{q}g}. \quad (2.19)$$

For  $i = q\bar{q}, gg$  we parameterize  $D_{RL,i}$  as follows:

$$D_{RL,i} = \frac{4\pi\alpha}{m_t^2} [\alpha \tilde{h}_i^{(0W, hel)}(\eta) + \alpha_s^2 \tilde{h}_i^{(1W, hel)}(\eta)], \quad (2.20)$$

where the order  $\alpha^2$  term is present only for  $i = q\bar{q}$ . As the SM amplitudes are CP-invariant to NLO in the weak interactions, Eq. (2.17) holds and we obtain the relations

$$\tilde{h}_{q\bar{q}}^{(0W, hel)} = h_{q\bar{q}}^{(0W, hel)}, \quad \tilde{h}_i^{(1W, hel)} = h_i^{(1W, hel)}, \quad i = q\bar{q}, gg, \quad (2.21)$$

where the  $h_{q\bar{q}}^{(0W, hel)}$ ,  $h_i^{(1W, hel)}$  are the scaling functions of the single-spin observable (2.8) in the helicity basis. For the  $q\bar{q}$  initial state they were given<sup>5</sup> in [21], and for  $gg$  fusion it is shown in Fig. 5.

The asymmetry  $D_{RL,i}$ , which for  $i = gg, q\bar{q}$  is invariant under a CP transformation, should not be confused with the following P- and CP-odd, but T-even spin asymmetry [42, 45]:

$$\langle\langle (2\mathbf{S}_t - 2\mathbf{S}_{\bar{t}}) \cdot \hat{\mathbf{k}} \rangle\rangle_i = 2\sigma_{i,++} - 2\sigma_{i,--}, \quad i = q\bar{q}, gg, \quad (2.22)$$

where the first (second) subscript refers to the  $t$  ( $\bar{t}$ ) helicity. A non-zero value of (2.22) – or equivalently, a violation of (2.17) – requires CP-violating absorptive parts in the scattering amplitude. These may be generated, for instance, by non-standard neutral Higgs bosons with both scalar and pseudoscalar couplings to top quarks [42, 41, 45].

For arbitrary reference axes  $\hat{\mathbf{a}}, \hat{\mathbf{b}}$  the analogue of (2.22) reads:

$$\langle\langle (2\mathbf{S}_t \cdot \hat{\mathbf{a}} + 2\mathbf{S}_{\bar{t}} \cdot \hat{\mathbf{b}}) \rangle\rangle_i = 2\sigma_i(\uparrow\uparrow) - 2\sigma_i(\downarrow\downarrow). \quad (2.23)$$

Finally we analyze the weak interaction contributions to parity- and T-even  $t\bar{t}$  spin-correlation observables, which are generated already to lowest order QCD. For the Tevatron these spin correlations (including NLO corrections) are largest with respect to the beam and off-diagonal bases, while for the LHC the helicity basis is a good choice<sup>6</sup>. In addition, as was shown in [15], a good measure for the spin correlation of the  $t\bar{t}$  pair produced at the LHC is the distribution of the opening angle between the two particles/jets from  $t$  and  $\bar{t}$  decay that are used as top-spin analyzers. A non-uniform distribution is due to

<sup>5</sup>The results for the single-spin scaling functions  $h_{q\bar{q}}$  given in [21] must be multiplied by a factor 2.

<sup>6</sup>For the LHC, a basis has been constructed [39] which gives a QCD effect which is somewhat larger than using the helicity correlation.

the correlation  $\mathbf{S}_t \cdot \mathbf{S}_{\bar{t}}$ . Within the SM these spin correlations result, for most values of the parton c. m. energy squared which are accessible at the Tevatron and at the LHC, almost exclusively from the strong interaction dynamics; the effect of the weak interactions on these observables turns out to be small. As the precise measurement of these correlations is expected to be feasible only at the LHC, we display here results only for two observables which are useful for data analysis at this collider. These are the helicity correlation and the spin-spin projection mentioned above, which we denote, using the convention of [21], by

$$O_3 \equiv -4(\hat{\mathbf{k}} \cdot \mathbf{S}_t)(\hat{\mathbf{k}} \cdot \mathbf{S}_{\bar{t}}), \quad (2.24)$$

$$O_4 \equiv 4\mathbf{S}_t \cdot \mathbf{S}_{\bar{t}} = 4 \sum_{i=1}^3 (\hat{\mathbf{e}}_i \cdot \mathbf{S}_t)(\hat{\mathbf{e}}_i \cdot \mathbf{S}_{\bar{t}}), \quad (2.25)$$

where  $\hat{\mathbf{k}}$  denotes as before the  $t$  direction in the  $t\bar{t}$  ZMF, and the factor 4 is conventional. The vectors  $\hat{\mathbf{e}}_{i=1,2,3}$  in (2.25) form an orthonormal basis. The unnormalized expectation values of these observables correspond to unnormalized double spin asymmetries, i.e., to the following combination of  $t, \bar{t}$  spin-dependent cross sections:

$$\langle\langle O_b \rangle\rangle_i = \sigma_i(\uparrow\uparrow) + \sigma_i(\downarrow\downarrow) - \sigma_i(\uparrow\downarrow) - \sigma_i(\downarrow\uparrow). \quad (2.26)$$

The arrows on the right-hand side refer to the spin state of the top and antitop quarks with respect to the reference axes  $\hat{\mathbf{a}}$  and  $\hat{\mathbf{b}}$ .

Again we compute the order  $\alpha_s^2\alpha$  weak contribution to (2.26) and express it in terms of scaling functions. For comparison we exhibit also the lowest order QCD term:

$$\langle\langle O_b \rangle\rangle_{gg} = \langle\langle O_b \rangle\rangle_{gg}^{(0)} + \langle\langle O_b \rangle\rangle_{gg}^W = \frac{4\pi}{m_t^2} [\alpha_s^2 g_{gg}^{(0,b)}(\eta) + \alpha_s^2 \alpha g_{gg}^{(1W,b)}(\eta)]. \quad (2.27)$$

The lowest order QCD and the weak contribution are plotted in Figs. 6 and 7 for  $b = 3, 4$ , respectively. The NLO QCD contributions to (2.27) were computed in [15]. A comparison of the LO and NLO QCD and of the weak contributions shows that, as far as the P-even spin correlations are concerned, the SM weak interaction effects are small in most of the  $t\bar{t}$  invariant mass range that is relevant for the LHC. A closer inspection will be made in the next section.

For completeness we remark that the absorptive parts of  $\delta\mathcal{M}_W$  lead to T-odd  $t\bar{t}$  spin correlations, both P-even and odd ones. These are very small effects, and we do not display them here.

### 3. Results for $pp$ ( $p\bar{p}$ ) collisions

Let us now investigate  $t\bar{t}$  production at the level of hadronic collisions. Before analyzing distributions, we first compute the weak corrections to the hadronic  $t\bar{t}$  cross section at the Tevatron and the LHC. Table 1 contains the contributions from  $gg \rightarrow t\bar{t}(g)$ , namely at NLO QCD (that is, the sum of the first two terms in Eq. (2.3)) and the weak corrections of order  $\alpha_s^2\alpha$ , while Table 2 contains the contributions from  $q\bar{q} \rightarrow t\bar{t}(g)$ , using the results for the weak corrections given in [21]. Notice that in this case the order  $\alpha^2$  Born contribution must not be neglected as compared to the  $\alpha_s^2\alpha$  term. Here we use the NLO parton distribution functions (PDF) CTEQ6.1M [35]. The Tables show that the weak interaction correction to

Table 1: The  $gg$ -induced hadronic  $t\bar{t}$  cross section at the Tevatron ( $\sqrt{s} = 1.96$  TeV) and at the LHC ( $\sqrt{s} = 14$  TeV) in units of pb, using the NLO parton distribution functions CTEQ6.1M [35],  $m_t = 172.7$  GeV, two values of the Higgs mass, and three different values of  $\mu$ . We put  $\mu \equiv \mu_R = \mu_F$ .

		$\mu = m_t/2$	$\mu = m_t$	$\mu = 2m_t$
Tevatron	NLO QCD	1.293	1.107	0.891
	weak			
	$m_H = 120$ GeV	-0.0176	-0.0111	-0.0073
	$m_H = 200$ GeV	-0.0212	-0.0135	-0.0090
LHC	NLO QCD	794.544	769.988	712.341
	weak			
	$m_H = 120$ GeV	-13.137	-10.095	-7.892
	$m_H = 200$ GeV	-13.511	-10.431	-8.198

Table 2: The  $q\bar{q}$ -induced hadronic  $t\bar{t}$  cross section at the Tevatron ( $\sqrt{s} = 1.96$  TeV) and at the LHC ( $\sqrt{s} = 14$  TeV) in units of pb, using the NLO parton distribution functions CTEQ6.1M [35],  $m_t = 172.7$  GeV,  $m_H = 120$  GeV, and three different values of  $\mu$ .

		$\mu = m_t/2$	$\mu = m_t$	$\mu = 2m_t$
Tevatron	NLO QCD	6.200	5.998	5.423
	weak	0.0515	0.0466	0.0419
LHC	NLO QCD	73.606	80.397	81.202
	weak	-0.990	-0.695	-0.476

the total cross section is negative at the LHC and amounts to about  $-1.3\%$ , while it is about  $0.5\%$  at the Tevatron. These contributions are much smaller than the scale uncertainties of the fixed-order NLO QCD corrections.

In the remaining section we study the weak interaction corrections for a number of distributions and compare them, in the case of P-invariant observables, with the lowest order QCD results. Therefore we compute these distributions with the LO parton distribution functions CTEQ6.L1 [35] which we take at the factorization scale  $\mu = 2m_t$ , and the input from the  $gg$  and  $q\bar{q}$  initiated subprocesses is evaluated with the values of the QCD and QED couplings given in the previous Section.

Figs. 8 and 9, left frames, show the weak corrections for the  $gg$  subprocess at the LHC, multiplied by  $-1$ , to the transverse top-momentum and to the  $t\bar{t}$  invariant mass distribution, together with the lowest order QCD results. We have compared our results Figs. 8 and 9 with those of [34] and we agree. Comparing with the results of [25] shown in Fig. 1 of that paper we disagree for  $p_T \sim 100$  GeV and  $M_{t\bar{t}} \sim 400$  GeV, where [25] finds  $d\sigma_{weak}$  to be positive below these values, while we obtain that  $d\sigma_{weak}$  is always negative for the  $gg$  subprocess and for  $m_H \gtrsim 120$  GeV.

Figs. 8 and 9, right frames, show the weak corrections for the  $q\bar{q}$  subprocesses at the LHC, multiplied

by  $-1$ , to the transverse top-momentum and to the  $t\bar{t}$  invariant mass distribution, together with the lowest order QCD results. The weak corrections consist of the  $O(\alpha^2)$   $q\bar{q} \rightarrow \gamma, Z \rightarrow t\bar{t}$  Born terms and the  $O(\alpha_s^2\alpha)$  virtual and real corrections to  $q\bar{q} \rightarrow t\bar{t}(g)$ . The latter corrections are separately infrared-divergent due to soft gluon radiation. We have computed these two distributions with our results of [21], where these divergences were treated with a phase-space slicing procedure, and we have checked that the sum of the virtual and real corrections of  $O(\alpha_s^2\alpha)$  are independent of the arbitrary slicing parameter  $x_{cut}$  if it is small enough. For  $p_T \lesssim 100$  GeV, respectively  $M_{t\bar{t}} \lesssim 430$  GeV, the weak corrections are positive for the  $q\bar{q}$  subprocesses. The size of the  $O(\alpha^2)$  Born terms, which are of course always positive, are between 10% and 20% of the  $O(\alpha_s^2\alpha)$  corrections in the  $M_{t\bar{t}}$  range considered, except in the vicinity of  $M_{t\bar{t}} \sim 450$  GeV, where the  $O(\alpha_s^2\alpha)$  corrections have a zero. Notice that, choosing  $m_H = 120$  (200) GeV, the weak  $q\bar{q}$  contributions are larger in magnitude than the ones from  $gg$  for  $p_T > 930$  (690) GeV.

Figs. 10 and 11 show the sum of the weak corrections to the transverse top-momentum and the  $t\bar{t}$  invariant mass distribution, together with the LO QCD results. Figs. 12 and 13 show the ratios  $[d\sigma_{weak}(gg)/dp_T]/[d\sigma_{LO}/dp_T]$ ,  $[d\sigma_{weak}(q\bar{q})/dp_T]/[d\sigma_{LO}/dp_T]$ , and the sum,  $[d\sigma_{weak}/dp_T]/[d\sigma_{LO}/dp_T]$  for the LHC, for two values of the Higgs mass, where  $d\sigma_I = d\sigma_I(gg + q\bar{q})$ ,  $I = weak, LO$ . The plots display clearly that the  $q\bar{q}$  part of the weak corrections is not negligible compared to those for the  $gg$  subprocess; as already mentioned, the  $q\bar{q}$  contributions dominate for large  $p_T$ . In Figs. 14 and 15 the analogous ratios are displayed for the  $M_{t\bar{t}}$  distribution. Notice that in these ratios the changes of  $d\sigma_{weak}$  and  $d\sigma_{LO}$  due to variations of the LO PDF and the LO QCD coupling with  $\mu$  cancel to a large extent.

Figs. 16 and 17 display the weak and LO QCD contributions to the  $p_T$  and  $M_{t\bar{t}}$  distribution for the Tevatron, and Figs. 18 and 19 show the corresponding ratios. Here the weak corrections become positive for  $p_T \lesssim 120$  GeV,  $M_{t\bar{t}} \lesssim 450$  GeV if  $m_H = 120$  GeV.

The weak corrections to the distributions grow for large  $p_T$  and  $M_{t\bar{t}}$  as compared to the lowest order QCD results. For the  $p_T$  distribution at the LHC the sum of the weak corrections amounts to about  $-10\%$  for  $p_T = 890$  (950) GeV for  $m_H = 120$  (200) GeV. The weak corrections are less pronounced in the  $M_{t\bar{t}}$  distribution: for  $M_{t\bar{t}} = 2$  TeV and  $m_H = 120$  GeV they are about  $-6\%$  as compared to the lowest order result. Table 3 contains, for the LHC and the Tevatron, the LO  $t\bar{t}$  cross section and the weak corrections for  $M_{t\bar{t}}$  and  $p_T$  larger than a selected set of values  $p_T^*$  and  $M_{t\bar{t}}^*$ , respectively. Furthermore the ratio  $r = weak/LO$  and the statistical significance  $S = |r|\sqrt{N_{event}}$  in standard deviations (s.d.) are tabulated assuming an integrated luminosity of  $10 \text{ fb}^{-1}$  for the Tevatron and  $100 \text{ fb}^{-1}$  for the LHC.

The numbers for  $S$  should be taken only as order of magnitude estimates because, as emphasized in the previous section, a precise determination  $r$  of these ratios must take the NLO QCD corrections into account, both near threshold and for large  $p_T$  or  $M_{t\bar{t}}$ , where these corrections are dominant. A definite statement about whether or not SM weak interaction effects are “visible” in distributions like  $d\sigma/dp_T$  and  $d\sigma/dM_{t\bar{t}}$  for large  $p_T$ ,  $M_{t\bar{t}}$  requires a reliable computation of  $d\sigma_{QCD}$  beyond the leading order, including resummation of gluon radiation [7, 8, 9, 10, 11] and a study of the renormalization and factorization scale uncertainties in that range. This is an important issue, especially at the LHC, as the  $M_{t\bar{t}}$  spectrum probes the existence of exotic heavy resonances that strongly couple to  $t\bar{t}$ , but is beyond the scope of this paper.

Next we consider two differential parity-conserving double spin asymmetries for the LHC which correspond to the spin-spin correlation observables  $O_3$  and  $O_4$  above. For brevity only the contribution from the  $gg$  subprocess will be taken into account, see [21] for the  $q\bar{q}$  contributions. The helicity correlation  $O_3$  leads to the asymmetry  $d\sigma_{++} + d\sigma_{--} - d\sigma_{+-} - d\sigma_{-+}$ , where as before the first (second) subscript

Table 3: Upper part: Cross section for  $t\bar{t}$  events with  $t\bar{t}$  invariant mass larger than  $M_{t\bar{t}}^*$  and for events with  $p_T > p_T^*$ . The rows contain the leading order QCD cross section and the weak corrections for two different Higgs boson masses in units of pb, the respective ratios  $r = \text{weak}/\text{LO}$  and the statistical significance  $S$  in s.d. assuming an integrated luminosity of  $10 \text{ fb}^{-1}$  for the Tevatron and  $100 \text{ fb}^{-1}$  for the LHC. The numbers for the LO cross section and the weak corrections given in the table were rounded, while  $r$  and  $S$  were computed with the precise numbers.

	$\sigma(M_{t\bar{t}} > M_{t\bar{t}}^*)$ [pb]							
	$M_{t\bar{t}}^*$ [GeV]	LO	weak, $m_H = 120 \text{ GeV}$	r [%]	S	weak, $m_H = 200 \text{ GeV}$	r [%]	S
LHC	500	174.7	-4.42	-2.5	105	-3.8	-2.2	90
	1000	10.7	-0.44	-4.1	42	-0.39	-3.7	38
	1500	1.39	-0.078	-5.6	21	-0.073	-5.2	19
Tev.	400	2.65	-0.01	-0.4	0.6	0.0009	0.03	0.05
	700	0.098	-0.0031	-3.2	1.0	-0.0023	-2.4	0.75
	1000	0.003	-0.00012	-4.5	0.23	-0.0001	-3.7	0.2

	$\sigma(p_T > p_T^*)$ [pb]							
	$p_T^*$ [GeV]	LO	weak, $m_H = 120 \text{ GeV}$	r [%]	S	weak, $m_H = 200 \text{ GeV}$	r [%]	S
LHC	200	59.8	-2.1	-3.5	85	-1.77	-3.0	72
	500	1.6	-0.12	-7.3	29	-0.11	-6.6	27
	1000	0.037	-0.0047	-12.8	7	-0.004	-12.2	7
Tev.	100	5.8	-0.016	-0.28	0.6	-0.007	-0.1	0.3
	200	0.71	-0.01	-1.4	1.2	-0.007	-1.0	0.8
	500	0.011	-0.00002	-0.23	0.02	-0.00002	-0.2	0.02

refers to the  $t$  ( $\bar{t}$ ) helicity. With  $N_g \equiv d\sigma(gg)/dM_{t\bar{t}}$ , where  $d\sigma(gg)$  denotes the LO QCD and the weak contributions for the  $gg$  subprocess, we consider

$$A_{hel} \equiv N_g^{-1} \left( \frac{d\sigma_{++}}{dM_{t\bar{t}}} + \frac{d\sigma_{--}}{dM_{t\bar{t}}} - \frac{d\sigma_{+-}}{dM_{t\bar{t}}} - \frac{d\sigma_{-+}}{dM_{t\bar{t}}} \right), \quad (3.1)$$

In complete analogy to  $A_{hel}$  we can define an asymmetry  $A_{spin}$  based on the spin-spin projection  $O_4$ . For numerical evaluation we decompose the numerator of (3.1) into the QCD Born and the weak contribution,  $A_{hel} = A_{hel}^{LO} + A_{hel}^{weak}$ . The same decomposition is made for  $A_{spin}$ . The two pieces are shown as functions of  $M_{t\bar{t}}$  for the helicity and spin asymmetry in Figs. 20 and 21, respectively. In Fig. 22 the ratio  $A_{hel}^{weak}/A_{hel}^{LO}$  is plotted. The corresponding ratio for  $A_{spin}$ , which is not displayed here, looks almost identical. Fig. 22 shows that the weak corrections are about  $-10\%$  of the Born term for  $M_{t\bar{t}} > 1 \text{ TeV}$ . Near  $M_{t\bar{t}} = 900 \text{ GeV}$ ,  $A_{hel}^{LO}$  has a zero. However, the NLO QCD corrections to these correlations, computed in [15], render  $A_{hel}^{QCD}$  non-zero at these values of  $M_{t\bar{t}}$ . For large  $M_{t\bar{t}}$  the NLO QCD corrections are the dominant contributions. Thus we conclude that the SM weak interaction contributions to parity-invariant double spin asymmetries at the LHC are quite small. Nevertheless, they should be taken into account in SM predictions in view of the estimated error of about 5% with which these asymmetries may be

measured [44].

The quantity  $A_{hel}$  and the ratio  $A_{hel}^{weak}/A_{hel}^{LO}$  was also computed in [23]. However, we disagree with the results given in Figs. 2 and 3 of that paper. While we obtain that  $A_{hel}^{weak}/A_{hel}^{LO} \lesssim -0.1$  for  $M_{t\bar{t}} \gtrsim 1.4$  TeV (c.f. Fig. 22), the corresponding result in [23] is much smaller in magnitude.

Finally we analyze the P-violating single and double top-spin asymmetries of Section 2 at the level of hadronic collisions. The double spin asymmetries (2.14) for the various parton initial states  $i$  lead to the differential asymmetry

$$\Delta(\uparrow\downarrow) \equiv N^{-1} \left( \frac{d\sigma(\uparrow\downarrow)}{dM_{t\bar{t}}} - \frac{d\sigma(\downarrow\uparrow)}{dM_{t\bar{t}}} \right), \quad (3.2)$$

where as above the first (second) arrow refers to the  $t$  ( $\bar{t}$ ) spin projection onto the reference axis  $\hat{\mathbf{a}}$  ( $\hat{\mathbf{b}}$ ), and

$$N \equiv \frac{d\sigma(gg)}{dM_{t\bar{t}}} + \frac{d\sigma(q\bar{q})}{dM_{t\bar{t}}}. \quad (3.3)$$

Here we take into account both the LO QCD and the weak contributions to  $N$ . The relations (2.15) for the subprocesses  $i$  imply that

$$2\Delta(\uparrow\downarrow) = N^{-1} \left( \frac{d\sigma(\uparrow, un) - d\sigma(\downarrow, un)}{dM_{t\bar{t}}} - \frac{d\sigma(un, \uparrow) - d\sigma(un, \downarrow)}{dM_{t\bar{t}}} \right), \quad (3.4)$$

holds at the level of hadronic collisions. Here the first and second (third and fourth) term on the right-hand side of (3.4) is the distribution of a  $t\bar{t}$  sample with  $t$  ( $\bar{t}$ ) polarization parallel and anti-parallel to  $\hat{\mathbf{a}}$  ( $\hat{\mathbf{b}}$ ) and  $\bar{t}$  ( $t$ ) quarks with both spin projections added. As already emphasized, Eq. (3.4) is simply a consequence of rotational invariance.

Now we choose the helicity axes (2.10). In this case we use the notation

$$Z_{RL} \equiv \frac{d\sigma_{+-}}{dM_{t\bar{t}}} - \frac{d\sigma_{-+}}{dM_{t\bar{t}}}, \quad \Delta_{RL} \equiv \frac{Z_{RL}}{N}. \quad (3.5)$$

Further we define the  $t$  and  $\bar{t}$  single spin asymmetries in the helicity basis:

$$Z_{hel} \equiv \frac{d\sigma_{+,un}}{dM_{t\bar{t}}} - \frac{d\sigma_{-,un}}{dM_{t\bar{t}}}, \quad \bar{Z}_{hel} \equiv \frac{d\sigma_{un,+}}{dM_{t\bar{t}}} - \frac{d\sigma_{un,-}}{dM_{t\bar{t}}}, \quad (3.6)$$

and

$$\Delta_{hel} \equiv \frac{Z_{hel}}{N}, \quad \bar{\Delta}_{hel} \equiv \frac{\bar{Z}_{hel}}{N}. \quad (3.7)$$

Next we derive the consequences of CP invariance for these spin observables. Let us first consider proton-antiproton collisions. If CP invariance holds then (2.8), (2.17), (2.18), (3.4), and the fact that  $p\bar{p}$  is a CP eigenstate in its c. m. frame imply the relations

$$\bar{Z}_{hel} = -Z_{hel}, \quad Z_{RL} = Z_{hel} = -\bar{Z}_{hel}, \quad \Delta_{RL} = \Delta_{hel} = -\bar{\Delta}_{hel}. \quad (3.8)$$

These relations hold also when CP-symmetric phase-space cuts are applied. CP relations analogous to (3.8) can of course also be derived for other, appropriately defined distributions. Eqs. (3.8) hold to NLO in the weak interactions.

What about proton-proton collisions at the LHC? As long as we take into account only  $gg$  and  $q\bar{q}$  initiated  $t\bar{t}$  production the relations (3.8) are of course fulfilled. The single spin asymmetries (2.13) shown in Fig. 4 for top-quark pair production by  $Z$  boson exchange in  $gq(\bar{q}) \rightarrow t\bar{t}q(\bar{q})$  lead to a violation of (3.8). This follows from the result  $\langle\langle 2\mathbf{S}_t \cdot \hat{\mathbf{k}} \rangle\rangle_{qg} \neq \langle\langle 2\mathbf{S}_t \cdot \hat{\mathbf{k}} \rangle\rangle_{\bar{q}g}$  and the CP relations (2.19). However, the parity-violating contributions from these reactions to  $Z_{hel}$  and  $\bar{Z}_{hel}$  are, for large  $M_{t\bar{t}}$ , small at the LHC, which we shall show now. Fig. 23 displays the contributions of the  $gg$ ,  $q\bar{q}$ ,  $qg$  and  $\bar{q}g$  subprocesses to  $Z_{hel}$  at the LHC. We recall that they are independent of the Higgs mass. The virtual and real order  $\alpha_s^2\alpha$  corrections to the  $q\bar{q}$  subprocesses were determined in [21] with a phase-space slicing procedure. The sum of these contributions to (3.6) is infrared-finite and independent of the slicing parameter, as it should. In Fig. 24 the ratio  $(-1)(Z_{hel} + \bar{Z}_{hel})/(Z_{hel} - \bar{Z}_{hel})$  is plotted as a function of  $M_{t\bar{t}}$ . The numerator receives contributions from the  $qg$  and  $\bar{q}g$  subprocesses only, while in the denominator all partonic subprocesses contribute. Around  $M_{t\bar{t}} \simeq 400$  GeV this ratio is of order one, as the contributions from  $gg$  and  $q\bar{q}$  tend to cancel each other, see Fig. 23. For larger  $M_{t\bar{t}}$  this ratio decreases rapidly in magnitude. With this result we find that  $\Delta_{hel} + \bar{\Delta}_{hel}$  is about one per mill or less in the whole  $M_{t\bar{t}}$  range; that is, the violation of the last relation of (3.8) at the LHC by SM weak interactions is very small.

As the contribution of the  $qg$  and  $\bar{q}g$  subprocesses is small, it has been omitted in the next plots. For the Tevatron  $Z_{hel}$  is shown in Fig. 25. The ratio  $\Delta_{hel}$  is displayed in Fig. 26 and 27 for the LHC and the Tevatron, respectively. This asymmetry depends on the Higgs mass via the denominator  $N$ ; however, in the chosen range of  $m_H$  this dependence is not visible in the plots. As discussed above, we have  $\Delta_{RL} = \Delta_{hel}$  for the Tevatron, and this relation holds also to very good approximation for the LHC within the SM. That is, for the LHC  $\Delta_{RL}$  is given by the solid line in Fig. 26.

A parity-violating double spin asymmetry proportional to  $\Delta_{RL}$  was considered in detail first in [27] for SM weak interactions to order  $\alpha_s^2\alpha$ , for a two-Higgs doublet model, and for the minimal supersymmetric extension of the SM. As far as SM weak interactions are concerned, several contributions were not taken into account in [27], namely, for  $q\bar{q}$  annihilation, the infrared-divergent box contributions and the corresponding real gluon radiation and, for  $gg$  fusion, the non-singlet neutral current contribution (which contributes to  $\sigma$ , see Section 2). The double-spin asymmetry  $\delta\mathcal{A}_{LR}(M_{t\bar{t}})$  considered in that paper and our  $\Delta_{RL}$  are normalized differently, and the PDF used in [27] are now outdated. For these reasons a precise numerical comparison of our results with those of [27] is difficult. Let us compare the results for the integrated asymmetry

$$A_{hel} \equiv \frac{\int (d\sigma_{+,un} - d\sigma_{-,un})}{\int d\sigma} \quad (3.9)$$

which is the integrated version of  $\Delta_{hel}$  or  $\Delta_{RL}$ , and which is equal to the quantity  $\mathcal{A}$  of [27]. For the LHC, using the cut  $p_T > 100$  GeV, the result of ref. [27] is  $|\mathcal{A}| = 0.5\%$ , while we obtain  $A_{hel} = 0.44\%$ . For the Tevatron, using the cut  $p_T > 20$  GeV, ref. [27] obtained  $|\mathcal{A}| = 0.04\%$ , while we get  $A_{hel} = -0.46\%$ .

The  $gg$  contribution to the parity-violating single spin asymmetry in the helicity basis were computed for the LHC also in [23]. The quantity  $AL_{tt}$  of that paper corresponds<sup>7</sup> to  $-Z_{hel}/[d\sigma(gg)/dM_{t\bar{t}}]$ . We disagree with the results shown in Figs. 2 and 3 of that paper.

Let us now discuss how these  $t$  and  $\bar{t}$  spin effects manifest themselves at the level of the top-quark decay products. Of the main  $t\bar{t}$  decay modes, that is, the all-jets, lepton + jets, and dilepton channels,

<sup>7</sup>The asymmetry  $APV \propto d\sigma_{--} - d\sigma_{++}$  in Eq. 1 of [23] is CP-odd and corresponds to  $-\Delta_{CP}$  of Eq. (3.19) below; i.e., its value is zero to order  $\alpha_s^2\alpha$  when taking only contributions from  $gg$  and  $q\bar{q}$  subprocesses into account.

probably only the latter two are useful for top-spin physics, as the former has large backgrounds. The  $t, \bar{t}$  polarizations and spin-spin correlations discussed above lead, through the parity-violating weak decays of these quark, to characteristic angular distributions and correlations among the final state particles/jets. According to the SM, in semileptonic top-quark decays the outgoing charged lepton is the best top-spin analyzer, while for non-leptonic top decays the resulting least-energetic non- $b$  jet is a good and experimentally acceptable choice [46]. Thus, for measuring  $t\bar{t}$  spin correlations at the Tevatron or LHC one may consider the reactions

$$p\bar{p}, pp \rightarrow t\bar{t} + X \rightarrow a(\mathbf{p}_+) + \bar{b}(\mathbf{p}_-) + X, \quad (3.10)$$

where  $a$  and  $\bar{b}$  denotes either a charged lepton ( $\ell = e, \mu$ ) or a jet from  $t$  and  $\bar{t}$  decay, respectively, and  $\mathbf{p}_+$  and  $\mathbf{p}_-$  denote the 3-momenta of these particles/jets in the respective  $t$  and  $\bar{t}$  rest frame<sup>8</sup>. One may now choose two polar vectors  $\hat{\mathbf{a}}$  and  $\hat{\mathbf{b}}$  as reference axes, determine the angles  $\theta_+ = \angle(\mathbf{p}_+, \hat{\mathbf{a}})$  and  $\theta_- = \angle(\mathbf{p}_-, \hat{\mathbf{b}})$  event by event, and consider the double distributions

$$\frac{1}{\sigma_{ab}} \frac{d\sigma}{d\cos\theta_+ d\cos\theta_-} = \frac{1}{4} (1 + B_+ \cos\theta_+ + B_- \cos\theta_- - C \cos\theta_+ \cos\theta_-), \quad (3.11)$$

where  $\sigma_{ab}$  is the cross section of the channel (3.10). The right-hand side of (3.11) is the a priori form of this distribution if no cuts were applied. In the presence of cuts the shape of the distribution will in general be distorted; nevertheless, one may use the bilinear form (3.11) as an estimator in fits to data. The coefficient  $C$  contains the information about the parity-even  $t\bar{t}$  spin correlations. These distributions were predicted for the Tevatron and the LHC in [14, 15] to NLO QCD for an number of reference axes, including the helicity axes (2.10), in which case the corresponding  $t\bar{t}$  spin correlation is described by  $O_3$ . It is straightforward to add to these NLO QCD results the weak interaction corrections given by the function  $4\pi\alpha_s^2\alpha_{gg}^{(1W,3)}/m_t^2$ , defined in (2.27) and shown in Fig. 6, using the formalism outlined in [15]. This remark applies also to the weak interaction corrections to  $O_4$ , which induces the opening angle distribution [15]  $\sigma_{ab}^{-1}d\sigma/d\cos\varphi = (1 - D\cos\varphi)/2$ , where  $\varphi = \angle(\mathbf{p}_+, \mathbf{p}_-)$ . Adding up all  $M_{t\bar{t}}$  bins the effect of the weak interaction corrections to  $C_{hel}$  and to  $D$  are not significantly larger than the estimated experimental error of about 4% at the LHC [44]. As discussed above the weak interaction contributions may be enhanced by suitable cuts on  $M_{t\bar{t}}$ .

The information about the parity-odd, T-even top spin effects – i.e., the single and double spin asymmetries (2.8), (2.14) – is contained in the coefficients  $B_{\pm}$  of (3.11). The highest sensitivity to these effects is achieved with events where the  $t$  or  $\bar{t}$  decay semileptonically. Consider the reactions

$$p\bar{p}, pp \rightarrow t\bar{t} + X \rightarrow \ell^+(\mathbf{p}_+) + X, \quad (3.12)$$

where  $\ell = e, \mu$ . Experimentally, the event selection should discriminate against single  $t$  production, which also contributes to the final state (3.12). Integrating (3.11) with respect to  $\cos\theta_-$  yields the distribution

$$\frac{1}{\sigma_{\ell}} \frac{d\sigma}{d\cos\theta_+} = \frac{1}{2} (1 + B_+ \cos\theta_+). \quad (3.13)$$

---

<sup>8</sup>For the lepton + jets and for the dileptonic channels the  $t$  and  $\bar{t}$  momenta, i.e., their rest frames can be kinematically reconstructed up to ambiguities which may be resolved with Monte Carlo methods using the matrix element of the reaction.

We consider here the helicity basis, which is the best choice for the LHC. Thus  $\theta_+ = \angle(\mathbf{p}_+, \hat{\mathbf{k}})$ , where  $\hat{\mathbf{k}}$  is the  $t$  quark direction in the  $t\bar{t}$  ZMF. For the computation of  $B_+$  we need the unnormalized decay density matrix  $\rho$  for  $t \rightarrow \ell^+ + X$ , integrated over all final-state variables, except  $\cos\theta_+$ . It is given by  $2\rho = \Gamma_\ell(I + \kappa_+ \boldsymbol{\sigma} \cdot \hat{\mathbf{p}}_+)$ , where  $\boldsymbol{\sigma}_i$  denote the Pauli matrices,  $\Gamma_\ell$  is the semileptonic decay width and  $\kappa_+$  is the top-spin analyzing power of  $\ell^+$ . In the SM  $\kappa_+ = 1$  to lowest order and  $\kappa_+ = 0.9984$  including the order  $\alpha_s$  QCD corrections. With this ingredient and with the results above we obtain

$$B_+ = \kappa_+ \frac{\int dM_{t\bar{t}} Z_{hel}(M_{t\bar{t}})}{\sigma_{t\bar{t}}}, \quad (3.14)$$

where  $Z_{hel}$  is defined in (3.6) and  $\sigma_{t\bar{t}}$  denotes the total  $t\bar{t}$  cross section. With the results for  $Z_{RL} = Z_{hel}$  displayed in Figs. 23 and Fig. 25 we obtain the SM prediction for the parity-violating distribution (3.13) for the LHC and the Tevatron given in Table 4. The distribution (3.13) leads to the asymmetry

$$A_{PV} \equiv \frac{N_+ - N_-}{N_+ + N_-} = \frac{B_+}{2} \quad (3.15)$$

where  $N_\pm$  is the number of events (3.12) with  $\cos\theta_+$  larger or smaller than zero. If CP invariance holds,  $A_{PV}$  is equal to  $A_{RL}$  defined in (3.9). The numbers for  $A_{PV}$  for events at the Tevatron and at the LHC with a  $t\bar{t}$  invariant mass larger than  $M_{t\bar{t}}^*$  are given in Table 4. The statistical significance  $S$  is estimated by  $S \simeq A_{PV} \sqrt{N_+ + N_-}$ , where the number of dileptonic  $\ell^+ \ell'^-$  ( $\ell = e, \mu, \tau$ ) and  $\ell^+ + \text{jets}$  events, which constitute a fraction of about 2/9 of all  $t\bar{t}$  events. It has been computed assuming an integrated luminosity of  $10 \text{ (fb)}^{-1}$  and  $100 \text{ (fb)}^{-1}$  for the Tevatron and the LHC, respectively. For the LHC one obtains  $S > 4$  for suitable cuts. It remains to be investigated with which precision  $A_{PV}$  can actually be measured by an LHC experiment.

Table 4: Standard Model prediction for the parity-violating asymmetry (3.15) for the Tevatron and the LHC, and the statistical significance  $S$ .

$M_{t\bar{t}}^* \text{ [GeV]}$	$A_{PV, \text{ Tevatron}}$	$S$	$M_{t\bar{t}}^* \text{ [GeV]}$	$A_{PV, \text{ LHC}}$	$S$
400	-0.0027	0.2	500	0.0028	5.4
700	-0.0030	0.04	1000	0.0077	3.7
1000	-0.0026	0.006	1500	0.011	1.9

If one uses events where the  $\bar{t}$  quarks have decayed semileptonically,

$$p\bar{p}, pp \rightarrow t\bar{t} + X \rightarrow \ell^-(\mathbf{p}_-) + X, \quad (3.16)$$

the analogue of (3.13) is

$$\frac{1}{\sigma_\ell} \frac{d\sigma}{d\cos\theta_-} = \frac{1}{2} (1 + B_- \cos\theta_-), \quad (3.17)$$

where  $\theta_- = \angle(\mathbf{p}_-, \hat{\mathbf{k}}_{\bar{t}})$ , and it is to be recalled that  $\hat{\mathbf{k}}_{\bar{t}} = -\hat{\mathbf{k}}$  in the  $t\bar{t}$  ZMF. CP invariance, which holds to the order of perturbation theory employed here, implies that the  $\bar{t}$  decay density matrix  $\bar{\rho}(\bar{t} \rightarrow \ell^-)$  is of the form  $2\bar{\rho} = \Gamma_\ell(I - \kappa_+ \boldsymbol{\sigma} \cdot \hat{\mathbf{p}}_-)$ . Using this and (3.8) we obtain

$$B_- = B_+. \quad (3.18)$$

The Standard Model predictions of Figs. 23, 25 and of Table 4 may be used as reference values in future searches for parity-violating effects in hadronic  $t\bar{t}$  production and decay. Apart from new physics effects in  $t\bar{t}$  production, also non-SM effects in top decay may influence the distributions (3.13), (3.17). As the charged-lepton coefficient  $\kappa_+$  is maximal in the SM, it may be decreased by new interactions. For instance, if  $t \rightarrow b\ell^+\nu_\ell$  would be solely mediated by the exchange of a charged Higgs boson then  $\kappa_b = 1$  and  $\kappa_+ < 1$ , which would lead to a smaller  $A_{PV}$ . Thus larger values of  $A_{PV}$  than those given in Table 4 would point towards non-SM parity violation in  $t\bar{t}$  production. Effects larger than those given in Table 4 are possible for instance in two-Higgs doublet or supersymmetric models if the new particles are not too heavy [27]. As to new physics effects in polarized semileptonic top decay mediated by  $W$  exchange, one should note the following: if these new interactions lead only to anomalous form factors in the  $tWb$  vertex, this would not change the lepton angular distribution [47, 48], i.e.  $\kappa_+$ , as long as these anomalous form factors are small. On the other hand the energy distribution  $d\Gamma/dE_\ell$ , which we did not use in our analysis, may change. For supersymmetric QCD corrections to the  $tWb$  vertex the deviations from the SM are, however, negligible [49].

For completeness, we briefly discuss a differential distribution which results from the  $gg$  and  $q\bar{q}$  CP asymmetries (2.22). It reads in the helicity basis:

$$\Delta_{CP} \equiv N^{-1} \left( \frac{d\sigma_{++}}{dM_{t\bar{t}}} - \frac{d\sigma_{--}}{dM_{t\bar{t}}} \right) = \frac{1}{2} (\Delta_{hel} + \bar{\Delta}_{hel}) . \quad (3.19)$$

The second equality is due to rotational invariance. As already emphasized this asymmetry is a probe of non-standard CP violation in  $t\bar{t}$  production. A non-zero value of  $\Delta_{CP}$  is equivalent to a violation of (3.8). In order to check for CP violation with this variable at the level of the top-quark decay products, one strategy would be to compare the distributions (3.13) and (3.17) for an event sample (3.12) and (3.16), respectively, i.e., to check for a violation of (3.18). If, for instance, non-standard heavy neutral Higgs boson(s)  $\phi$  with mass  $m_\phi \gtrsim 2m_t$  and with scalar and pseudoscalar Yukawa couplings to top quarks exist,  $\Delta_{CP}$  and likewise  $B_+ - B_-$  can be of the order of several percent in magnitude around  $M_{t\bar{t}} \sim m_\phi$  as was shown in [43]. As discussed above, at the LHC there are SM contributions to (3.19) from the  $qg$  and  $\bar{q}g$  subprocesses, but this amounts to less than one per mill.

## 4. Conclusions

The main interest in the SM weak interaction corrections to hadronic  $t\bar{t}$  production is the determination of their size at large transverse top-momentum and/or large  $t\bar{t}$  invariant mass (i.e., the weak Sudakov effects) and of the parity-violating effects, especially at the LHC. In this paper we have calculated the one-loop weak corrections to top quark pair production due to gluon-gluon fusion and (anti)quark-gluon scattering. This gives, together with our previous result for  $q\bar{q} \rightarrow t\bar{t}(g)$  [21], the complete corrections of order  $\alpha_s^2\alpha$  to  $t\bar{t}$  production with  $t$  and  $\bar{t}$  polarizations and spin-correlations fully taken into account. For  $t\bar{t}$  production at the Tevatron and at LHC we have determined the weak contributions to the transverse top-momentum and to the  $t\bar{t}$  invariant mass distributions. For the LHC the size of the weak corrections to  $d\sigma/dp_T$  and  $d\sigma/dM_{t\bar{t}}$  is of the order of 10 percent for large  $p_T$  and  $M_{t\bar{t}}$ , respectively, as compared with LO results. Further we have computed the order  $\alpha_s^2\alpha$  contributions to two parity-even  $t\bar{t}$  spin correlation observables which are of interest for the LHC. As far as parity-violating effects are concerned

we derived, for CP-invariant interactions, relations between parity-violating double and single top spin asymmetries. We pointed out how one may probe in this context for non-standard CP violation, and we computed the SM background to an appropriate observable for the LHC. The parity-violating effects are best analyzed for  $t\bar{t}$  events where the  $t$  ( $\bar{t}$ ) quark decays semileptonically, and we have computed a charged-lepton forward-backward asymmetry  $A_{PV}$  with respect to the  $t$  ( $\bar{t}$ ) quark direction. At the LHC  $A_{PV}$  is of the order of one percent for suitable cuts on  $M_{t\bar{t}}$ . Whether such a small asymmetry can be measured at the LHC remains to be investigated by experimentalists with simulations including detector effects. Nevertheless, this result should serve, like the predictions for  $d\sigma_{weak}/dp_T$  and  $d\sigma_{weak}/dM_{t\bar{t}}$ , as a reference in the detailed exploration of the top quark interactions with future data.

### Acknowledgements

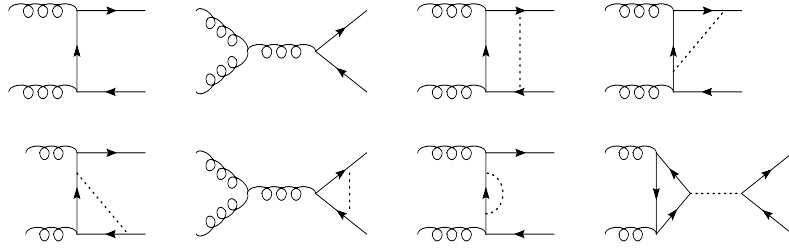
We thank A. Scharf and P. Uwer for discussions and for communication of their results prior to publication. Further we thank S. Moretti and D. Ross for a correspondence concerning [23]. W.B. wishes to thank also the Physics Department of Shandong University, Jinan, where part of this work was done, for its hospitality. This work was supported by Deutsche Forschungsgemeinschaft (DFG) SFB/TR9, by DFG-Graduiertenkolleg RWTH Aachen, by NSFC, by NCET, and by Huoyingdong Foundation, China.

## References

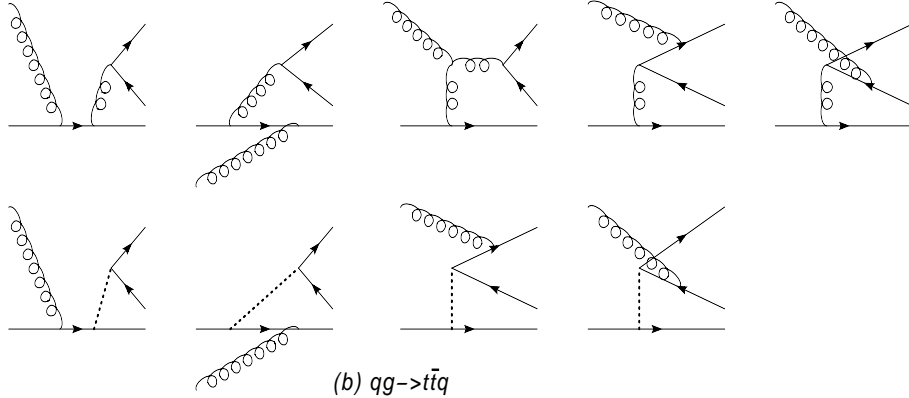
- [1] P. Nason, S. Dawson and R. K. Ellis, Nucl. Phys. B **303**, 607 (1988).
- [2] P. Nason, S. Dawson and R. K. Ellis, Nucl. Phys. B **327**, 49 (1989). [Erratum-ibid. B **335**, 260 (1990)].
- [3] W. Beenakker, H. Kuijf, W. L. van Neerven and J. Smith, Phys. Rev. D **40**, 54 (1989).
- [4] W. Beenakker, W. L. van Neerven, R. Meng, G. A. Schuler and J. Smith, Nucl. Phys. B **351**, 507 (1991).
- [5] M. L. Mangano, P. Nason and G. Ridolfi, Nucl. Phys. B **373**, 295 (1992).
- [6] S. Frixione, M. L. Mangano, P. Nason and G. Ridolfi, Phys. Lett. B **351**, 555 (1995) [arXiv:hep-ph/9503213].
- [7] R. Bonciani, S. Catani, M. L. Mangano and P. Nason, Nucl. Phys. B **529**, 424 (1998) [arXiv:hep-ph/9801375].
- [8] N. Kidonakis, E. Laenen, S. Moch and R. Vogt, Phys. Rev. D **64**, 114001 (2001) [arXiv:hep-ph/0105041].
- [9] M. Cacciari, S. Frixione, M. L. Mangano, P. Nason and G. Ridolfi, JHEP **0404**, 068 (2004) [arXiv:hep-ph/0303085].
- [10] N. Kidonakis and R. Vogt, Int. J. Mod. Phys. A **20**, 3171 (2005) [arXiv:hep-ph/0410367]; N. Kidonakis, Phys. Rev. D **68**, 114014 (2003) [arXiv:hep-ph/0308222].
- [11] A. Banfi and E. Laenen, Phys. Rev. D **71**, 034003 (2005) [arXiv:hep-ph/0411241].
- [12] W. Bernreuther, A. Brandenburg and Z. G. Si, Phys. Lett. B **483**, 99 (2000) [arXiv:hep-ph/0004184].
- [13] W. Bernreuther, A. Brandenburg, Z. G. Si and P. Uwer, Phys. Lett. B **509**, 53 (2001) [arXiv:hep-ph/0104096].
- [14] W. Bernreuther, A. Brandenburg, Z. G. Si and P. Uwer, Phys. Rev. Lett. **87**, 242002 (2001) [arXiv:hep-ph/0107086].
- [15] W. Bernreuther, A. Brandenburg, Z. G. Si and P. Uwer, Nucl. Phys. B **690**, 81 (2004) [arXiv:hep-ph/0403035].
- [16] M. Melles, Phys. Rept. **375**, 219 (2003) [arXiv:hep-ph/0104232].
- [17] A. Denner and S. Pozzorini, Eur. Phys. J. C **18**, 461 (2001) [arXiv:hep-ph/0010201]; Eur. Phys. J. C **21**, 63 (2001) [arXiv:hep-ph/0104127].
- [18] A. Denner, B. Jantzen and S. Pozzorini, arXiv:hep-ph/0608326.

- [19] W. Beenakker, A. Denner, W. Hollik, R. Mertig, T. Sack and D. Wackerroth, Nucl. Phys. B **411**, 343 (1994).
- [20] C. Kao, G. A. Ladinsky and C. P. Yuan, Int. J. Mod. Phys. A **12**, 1341 (1997).
- [21] W. Bernreuther, M. Fückler and Z. G. Si, Phys. Lett. B **633**, 54 (2006) [arXiv:hep-ph/0508091].
- [22] J. H. Kühn, A. Scharf and P. Uwer, Eur. Phys. J. C **45**, 139 (2006) [arXiv:hep-ph/0508092].
- [23] S. Moretti, M. R. Nolten and D. A. Ross, Phys. Lett. B **639**, 513 (2006) [arXiv:hep-ph/0603083].
- [24] E. Maina, S. Moretti, M. R. Nolten and D. A. Ross, Phys. Lett. B **570**, 205 (2003) [arXiv:hep-ph/0307021].
- [25] S. Moretti, M. R. Nolten and D. A. Ross, arXiv:hep-ph/0606201.
- [26] C. Kao, Phys. Lett. B **348**, 155 (1995) [arXiv:hep-ph/9411337].
- [27] C. Kao and D. Wackerroth, Phys. Rev. D **61**, 055009 (2000) [arXiv:hep-ph/9902202].
- [28] M. Beccaria, F. M. Renard and C. Verzegnassi, Phys. Rev. D **72**, 093001 (2005) [arXiv:hep-ph/0506230].
- [29] C. S. Li, C. P. Yuan and H. Y. Zhou, Phys. Lett. B **424**, 76 (1998) [arXiv:hep-ph/9709275].
- [30] W. Hollik, W. M. Möhle and D. Wackerroth, Nucl. Phys. B **516**, 29 (1998) [arXiv:hep-ph/9706218].
- [31] M. Beccaria, S. Bentvelsen, M. Cöbol, F. M. Renard and C. Verzegnassi, Phys. Rev. D **71**, 073003 (2005) [arXiv:hep-ph/0412249].
- [32] [LEP Collaborations], arXiv:hep-ex/0412015.
- [33] The Tevatron Electroweak Working Group, J.F. Arguin et al., arXiv:hep-ex/0507091.
- [34] J. H. Kühn, A. Scharf and P. Uwer, arXiv:hep-ph/0610335.
- [35] J. Pumplin, D. R. Stump, J. Huston, H. L. Lai, P. Nadolsky and W. K. Tung, JHEP **0207**, 012 (2002) [arXiv:hep-ph/0201195].
- [36] W. Bernreuther, A. Brandenburg and P. Uwer, Phys. Lett. B **368**, 153 (1996) [arXiv:hep-ph/9510300].
- [37] W. G. D. Dharmaratna and G. R. Goldstein, Phys. Rev. D **53**, 1073 (1996).
- [38] G. Mahlon and S. Parke, Phys. Lett. B **411**, 173 (1997) [arXiv:hep-ph/9706304].
- [39] P. Uwer, Phys. Lett. B **609**, 271 (2005) [arXiv:hep-ph/0412097].
- [40] W. Bernreuther, M. Flesch and P. Haberl, Phys. Rev. D **58**, 114031 (1998) [arXiv:hep-ph/9709284].

- [41] W. Bernreuther and A. Brandenburg, *Phys. Rev. D* **49**, 4481 (1994) [arXiv:hep-ph/9312210].
- [42] W. Bernreuther and A. Brandenburg, *Phys. Lett. B* **314**, 104 (1993).
- [43] W. Bernreuther, A. Brandenburg and M. Flesch, arXiv:hep-ph/9812387.
- [44] F. Hubaut, E. Monnier, P. Pralavorio, K. Smolek and V. Simak, *Eur. Phys. J. C* **44S2**, 13 (2005) [arXiv:hep-ex/0508061].
- [45] C. R. Schmidt and M. E. Peskin, *Phys. Rev. Lett.* **69**, 410 (1992).
- [46] A. Brandenburg, Z. G. Si and P. Uwer, *Phys. Lett. B* **539**, 235 (2002) [arXiv:hep-ph/0205023].
- [47] B. Grzadkowski and Z. Hioki, *Phys. Lett. B* **476**, 87 (2000) [arXiv:hep-ph/9911505].
- [48] S. D. Rindani, *Pramana* **54**, 791 (2000) [arXiv:hep-ph/0002006].
- [49] A. Brandenburg and M. Maniatis, *Phys. Lett. B* **545**, 139 (2002) [arXiv:hep-ph/0207154].



(a)  $gg \rightarrow t\bar{t}$



(b)  $qg \rightarrow t\bar{t}q$

Figure 1: (a) Lowest order QCD diagrams and 1-loop weak corrections to  $gg \rightarrow t\bar{t}$ . Crossed diagrams are not drawn. The dotted line in the box diagram and in the vertex and self-energy corrections represents  $W$ ,  $Z$  bosons, the corresponding Goldstone bosons, and the Higgs boson  $H$ . The fermion triangle in the last diagram represents a  $t$  and  $b$  quark loop, followed by  $s$  channel exchange of the  $Z$  boson, the associated Goldstone boson, and the Higgs boson. (b) Tree-level diagrams for  $qg \rightarrow t\bar{t}q$ . Upper row: QCD diagrams; lower row: mixed electroweak-QCD contributions. The dotted line represents a photon or a  $Z$  boson.

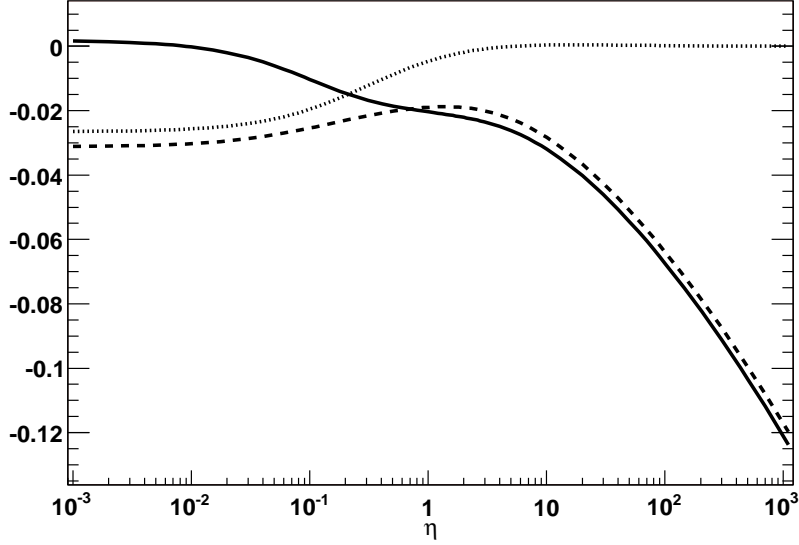


Figure 2: Ratio  $r_W^{(0)}$  of the order  $\alpha\alpha_s^2$  corrections and the Born cross section for  $gg \rightarrow t\bar{t}$  as a function of  $\eta$ , for two Higgs masses,  $m_H = 120$  GeV (solid) and  $m_H = 200$  GeV (dashed). The dotted curve shows the non-singlet neutral current contribution to  $r_W^{(0)}$ .

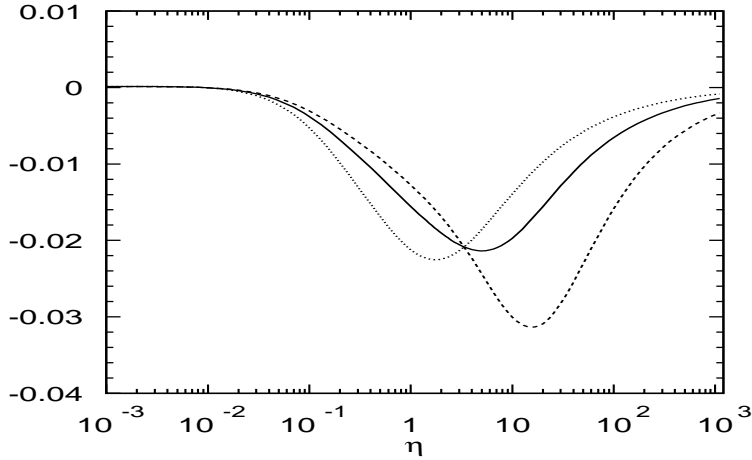


Figure 3: Ratio  $r_W^{(1)}$  of the order  $\alpha\alpha_s^2$  corrections (for  $m_H = 120$  GeV) and the NLO QCD cross section for  $gg \rightarrow t\bar{t}$  (taken from [13, 15]), evaluated for  $\mu = m_t/2$  (dotted),  $\mu = m_t$  (solid), and  $\mu = 2m_t$  (dashed).

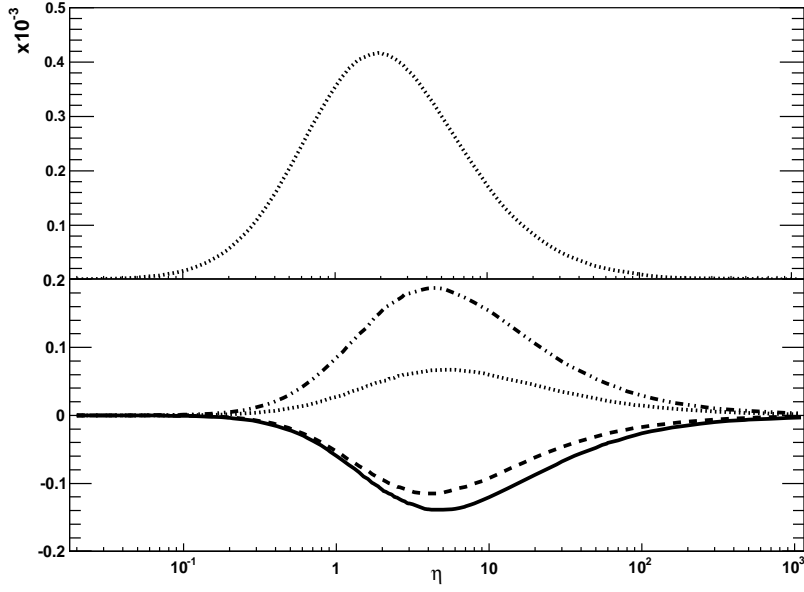


Figure 4: Upper frame: Scaling function  $f_{ug}^{(1W)}$  defined in (2.7) for u-type quarks. For d-type quarks,  $f_{dg}^{(1W)} = -f_{ug}^{(1W)}$ . Lower frame: Scaling functions  $h_{ug}^{(1W, hel)}$  (dotted),  $h_{dg}^{(1W, hel)}$  (solid),  $h_{\bar{u}g}^{(1W, hel)}$  (dashed), and  $h_{\bar{d}g}^{(1W, hel)}$  (dash-dotted) that determine the expectation value (2.13) for the helicity axis.

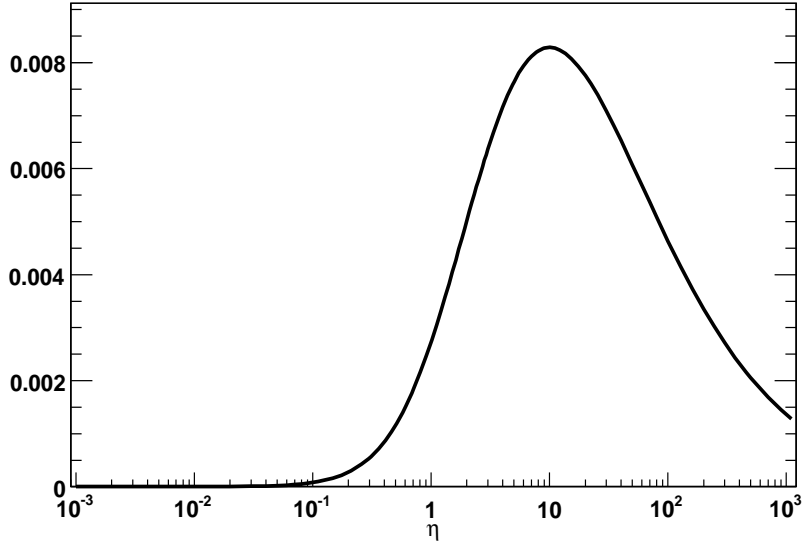


Figure 5: Scaling function  $h_{gg}^{(1W, hel)}$  that determines the expectation value (2.12) for the helicity axis.

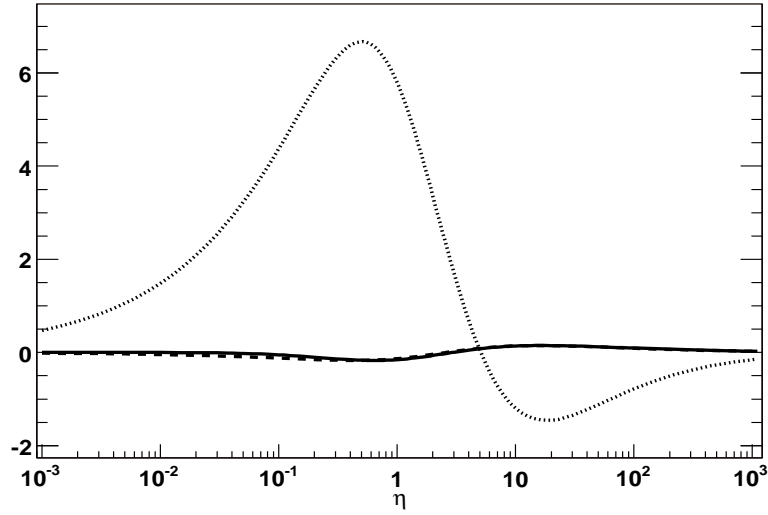


Figure 6: Unnormalized helicity correlation  $\langle\langle O_3 \rangle\rangle_{gg}$ , defined in (2.27), in units of [pb]. The dotted line is the lowest order QCD contribution, and the solid and dashed line is the weak contribution for  $m_H = 120$  GeV and  $m_H = 200$  GeV, respectively.

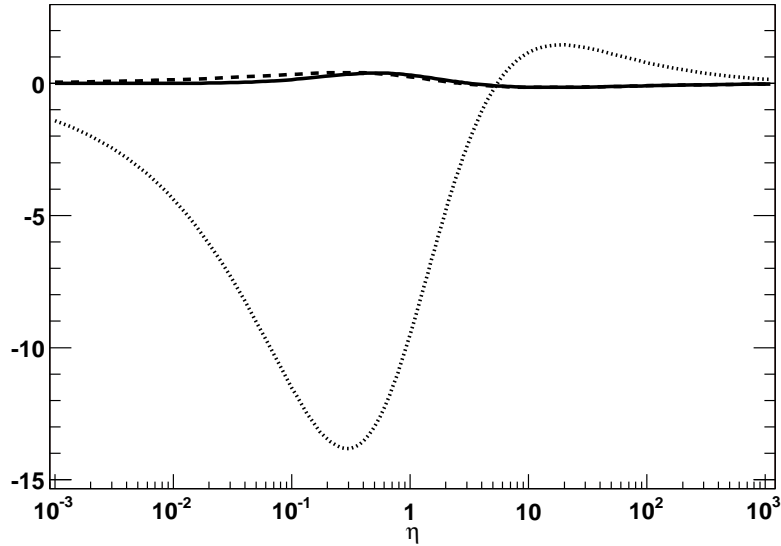


Figure 7: Unnormalized spin correlation  $\langle\langle O_4 \rangle\rangle_{gg}$ , defined in (2.27), in units of [pb]. The dotted line is the lowest order QCD contribution, and the solid and dashed line is the weak contribution for  $m_H = 120$  GeV and  $m_H = 200$  GeV, respectively.

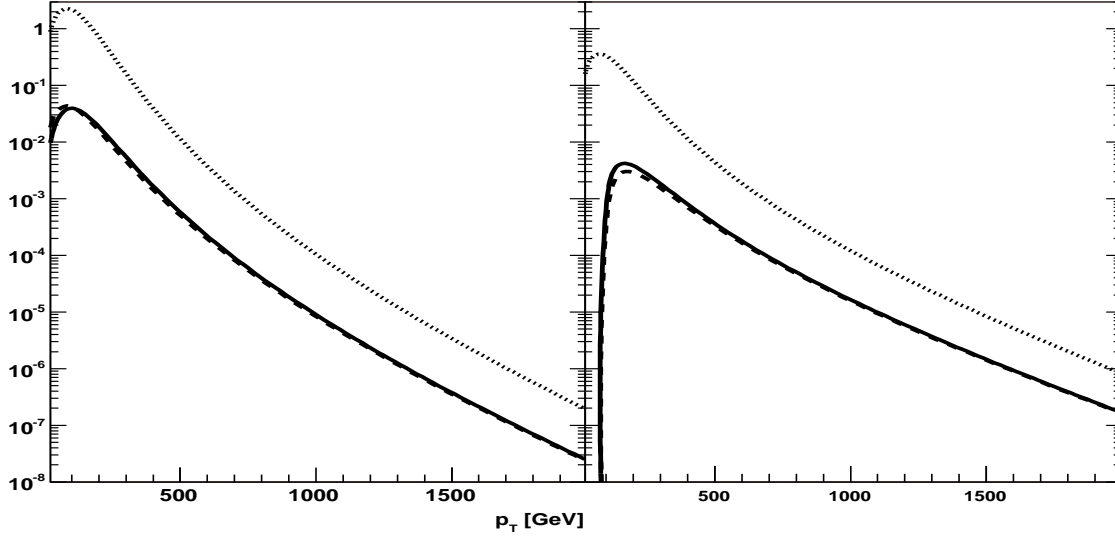


Figure 8: Left frame: Contributions to the transverse top-momentum distribution  $d\sigma(gg)/dp_T$  at the LHC due to the  $gg$  subprocess in units of [pb/GeV]. The dotted line is due to lowest order QCD, and the solid and dashed line is the weak correction multiplied by -1 for  $m_H = 120$  GeV and  $m_H = 200$  GeV, respectively. Right frame: The same for the  $q\bar{q}$  process.

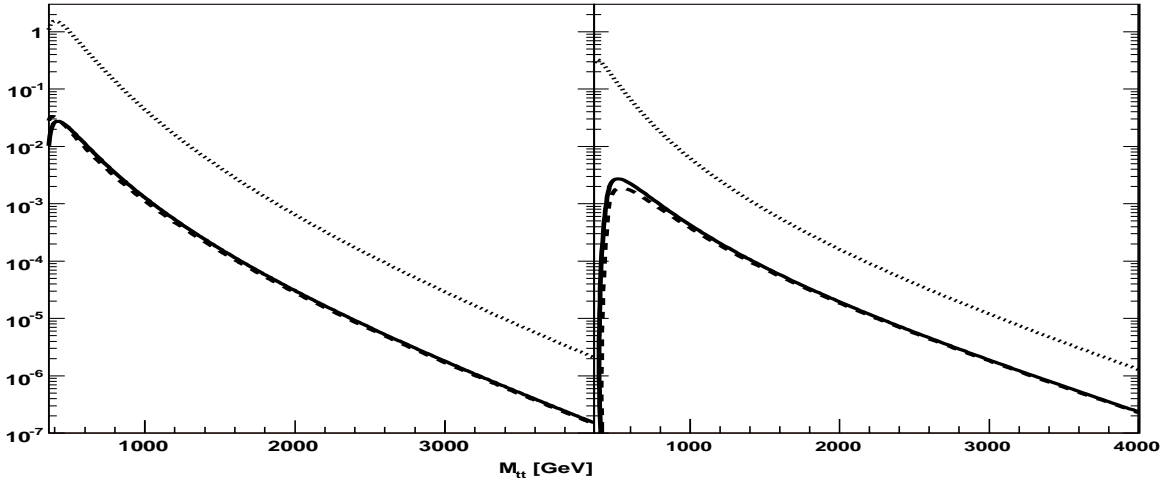


Figure 9: Left frame: Contributions to the invariant mass distribution  $d\sigma(gg)/dM_{t\bar{t}}$  at the LHC due to the  $gg$  subprocess in units of [pb/GeV]. The dotted line is due to lowest order QCD, and the solid and dashed line is the weak correction multiplied by -1 for  $m_H = 120$  GeV and  $m_H = 200$  GeV, respectively. Right frame: The same for the  $q\bar{q}$  subprocesses.

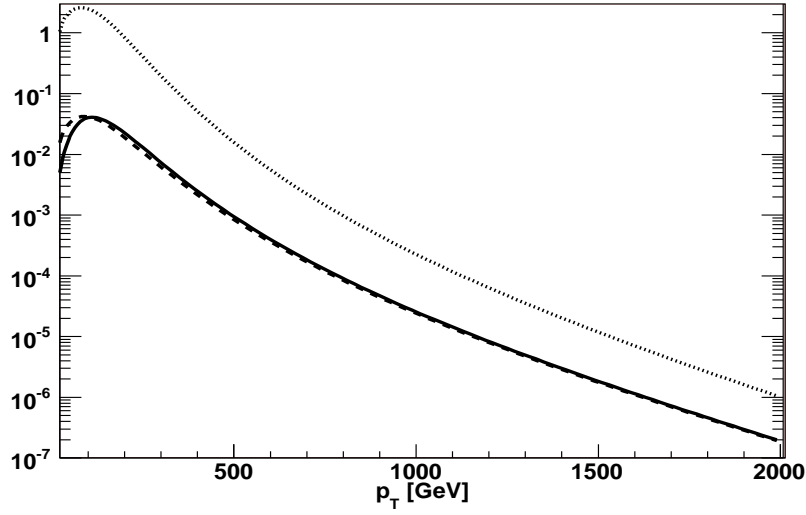


Figure 10: Contributions to the transverse momentum distribution  $d\sigma(gg + q\bar{q})/dp_T$  at the LHC due to the  $gg$  and  $q\bar{q}$  subprocesses in units of [pb/GeV]. The dotted line is due to lowest order QCD, and the solid and dashed line is the weak contribution multiplied by -1 for  $m_H = 120$  GeV and  $m_H = 200$  GeV, respectively.

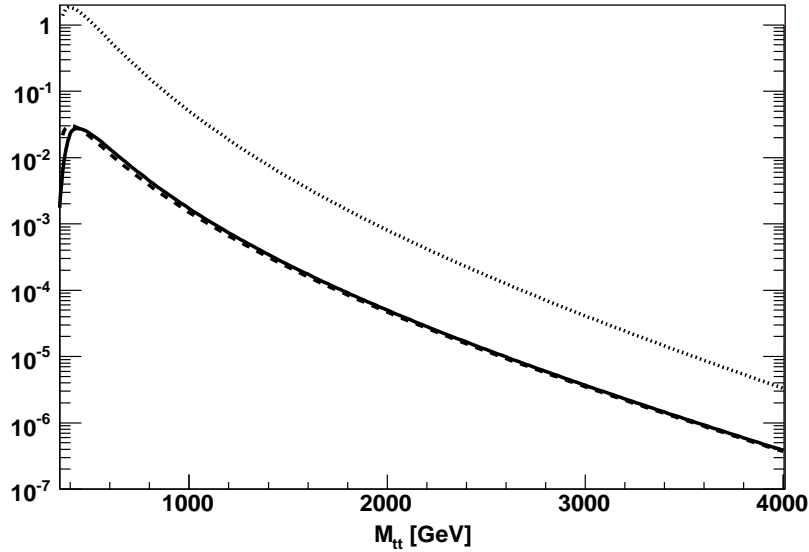


Figure 11: Contributions to the invariant mass distribution  $d\sigma(gg + q\bar{q})/dM_{t\bar{t}}$  at the LHC due to the  $gg$  and  $q\bar{q}$  subprocesses in units of [pb/GeV]. The dotted line is due to lowest order QCD, and the solid and dashed line is the weak contribution multiplied by -1 for  $m_H = 120$  GeV and  $m_H = 200$  GeV, respectively.

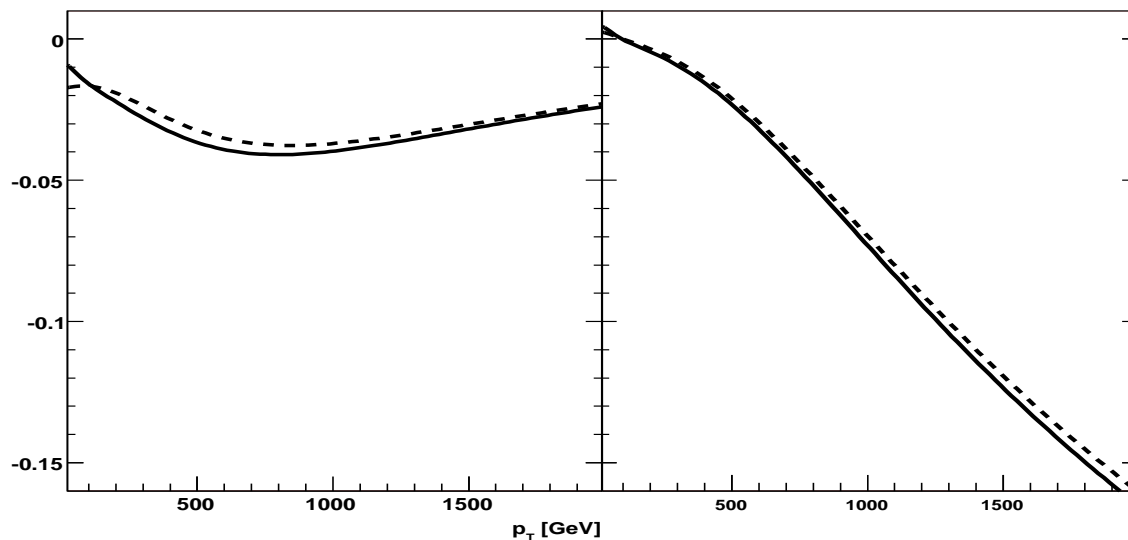


Figure 12: Ratios of  $d\sigma_{weak}(gg)/dp_T$  (left frame),  $d\sigma_{weak}(q\bar{q})/dp_T$  (right frame) and  $d\sigma_{LO}(gg + q\bar{q})/dp_T$  at the LHC. The solid and dashed line is for  $m_H = 120$  GeV and  $m_H = 200$  GeV, respectively.

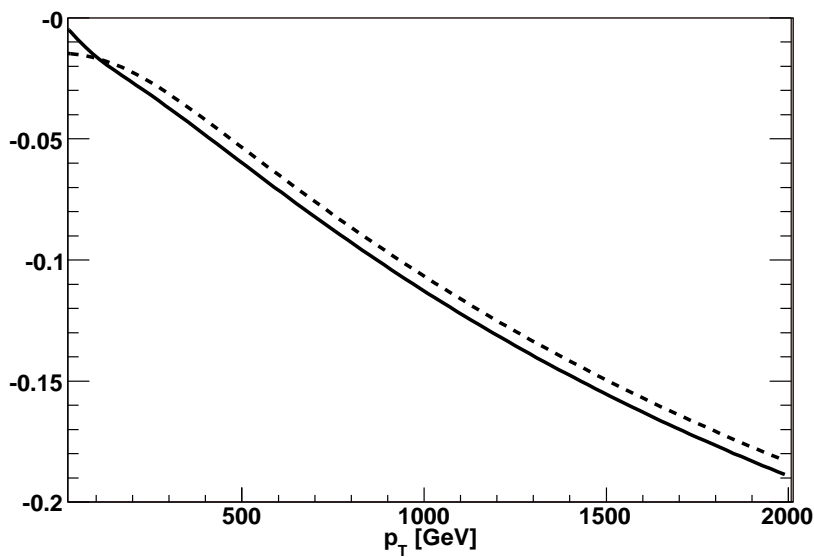


Figure 13: Ratio of  $d\sigma_{weak}(gg + q\bar{q})/dp_T$  and  $d\sigma_{LO}(gg + q\bar{q})/dp_T$  at the LHC. The solid and dashed line is for  $m_H = 120$  GeV and  $m_H = 200$  GeV, respectively.

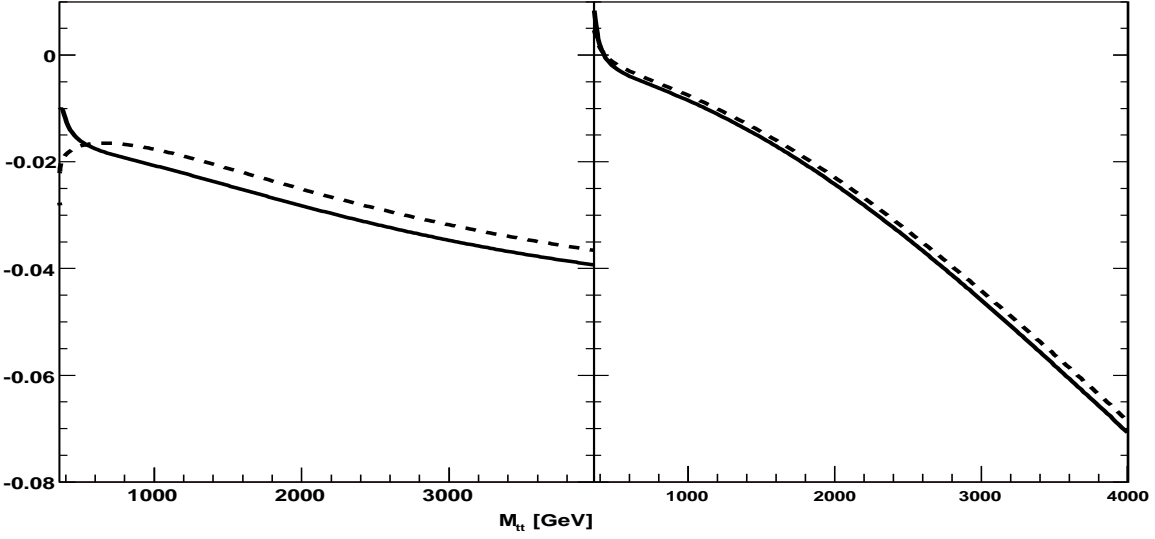


Figure 14: Ratios of  $d\sigma_{weak}(gg)/dM_{t\bar{t}}$  (left frame),  $d\sigma_{weak}(q\bar{q})/dM_{t\bar{t}}$  (right frame) and  $d\sigma_{LO}(gg + q\bar{q})/dM_{t\bar{t}}$  at the LHC. The solid and dashed line is for  $m_H = 120$  GeV and  $m_H = 200$  GeV, respectively.

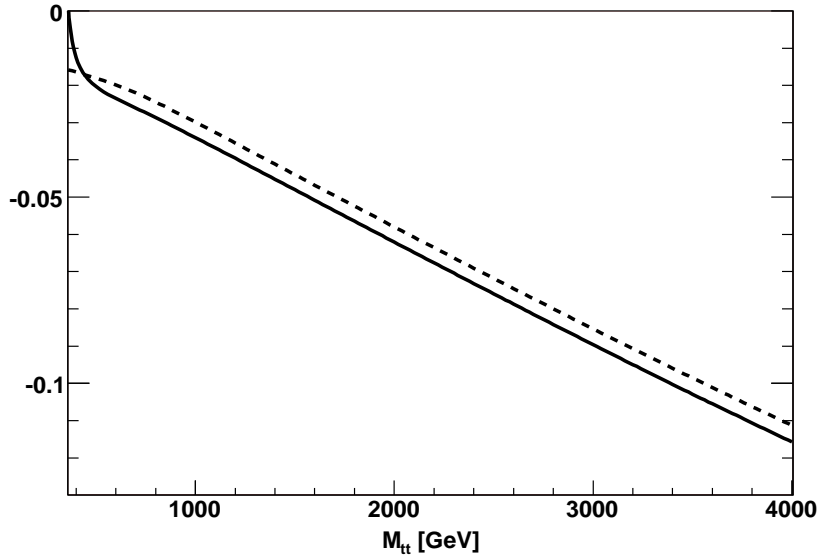


Figure 15: Ratio of  $d\sigma_{weak}(gg + q\bar{q})/dM_{t\bar{t}}$  and  $d\sigma_{LO}(gg + q\bar{q})/dM_{t\bar{t}}$  at the LHC. The solid and dashed line is for  $m_H = 120$  GeV and  $m_H = 200$  GeV, respectively.

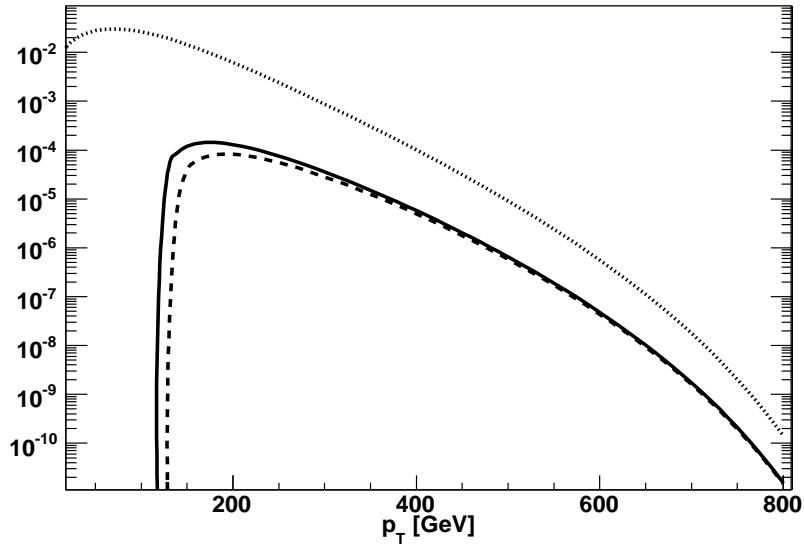


Figure 16: Contributions to the transverse momentum distribution  $d\sigma(gg + q\bar{q})/dp_T$  at the Tevatron due to the  $gg$  and  $q\bar{q}$  subprocesses in units of [pb/GeV]. The dotted line is due to lowest order QCD, and the solid and dashed line is the weak contribution multiplied by -1 for  $m_H = 120$  GeV and  $m_H = 200$  GeV, respectively.

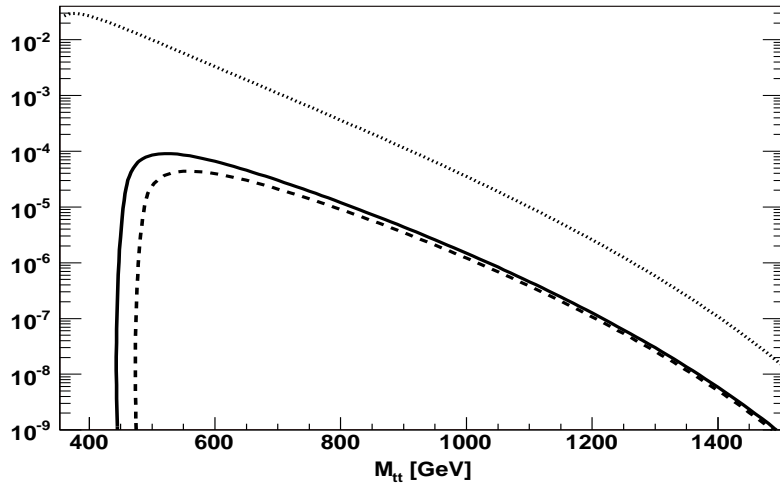


Figure 17: Contributions to the invariant mass distribution  $d\sigma(gg + q\bar{q})/dM_{t\bar{t}}$  at the Tevatron due to the  $q\bar{q}$  and  $gg$  subprocesses in units of [pb/GeV]. The dotted line is due to lowest order QCD, and the solid and dashed line is the weak contribution multiplied by -1 for  $m_H = 120$  GeV and  $m_H = 200$  GeV, respectively.

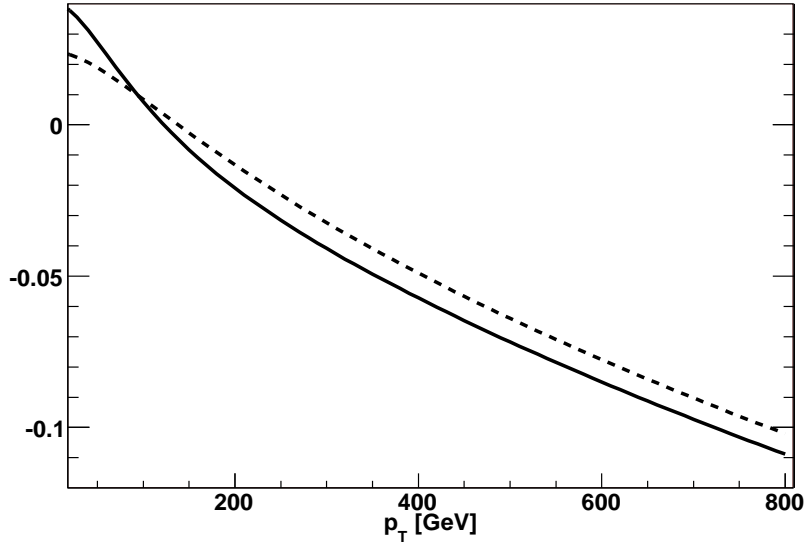


Figure 18: Ratio of the distributions  $(d\sigma/dp_T)_{weak}$  and  $(d\sigma/dp_T)_{LO,QCD}$ , shown in Fig. 16, at the Tevatron for  $m_H = 120$  GeV (solid) and  $m_H = 200$  GeV (dashed).

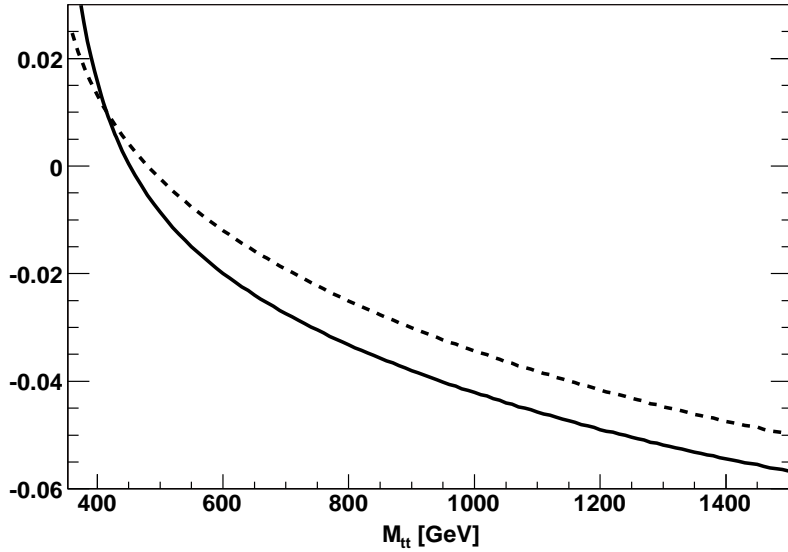


Figure 19: Ratio of  $d\sigma_{weak}(gg + q\bar{q})/dM_{t\bar{t}}$  and  $d\sigma_{LO}(gg + q\bar{q})/dM_{t\bar{t}}$ , shown in Fig. 17, at the Tevatron. The solid and dashed line is for  $m_H = 120$  GeV and  $m_H = 200$  GeV, respectively.

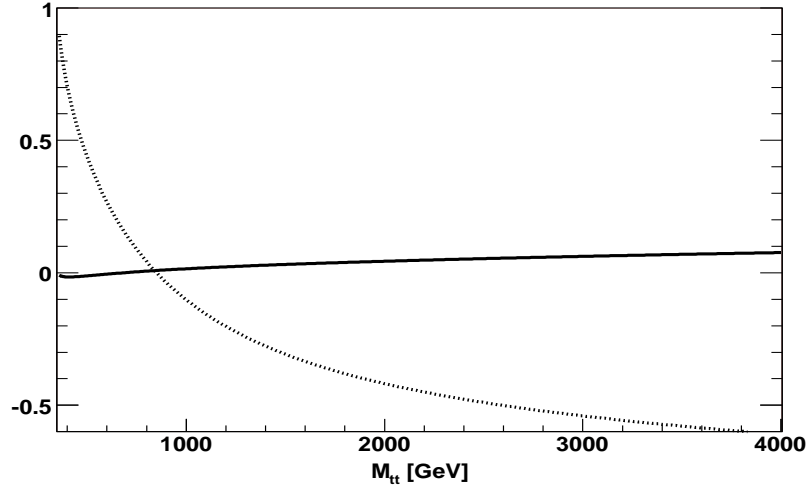


Figure 20: The P-invariant differential double spin asymmetry  $A_{hel}$ , defined in (3.1), at the LHC ( $gg$  subprocess only). The dotted and solid line is the contribution from lowest order QCD and from weak interactions with  $m_H = 120$  GeV, respectively. Using  $m_H = 200$  GeV does not lead to a significant change of the solid line.

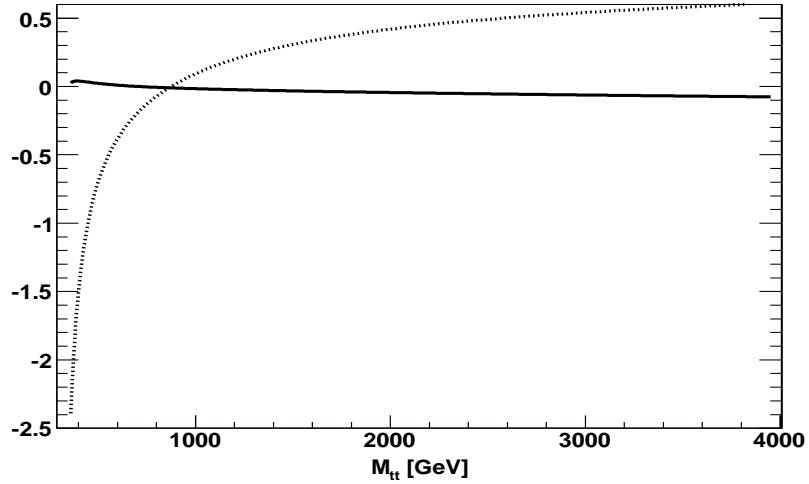


Figure 21: The P-invariant differential double spin asymmetry  $A_{spin}$  at the LHC ( $gg$  subprocess only). The dotted and solid line is the contribution from lowest order QCD and from weak interactions with  $m_H = 120$  GeV, respectively. Using  $m_H = 200$  GeV does not lead to a significant change of the solid line.

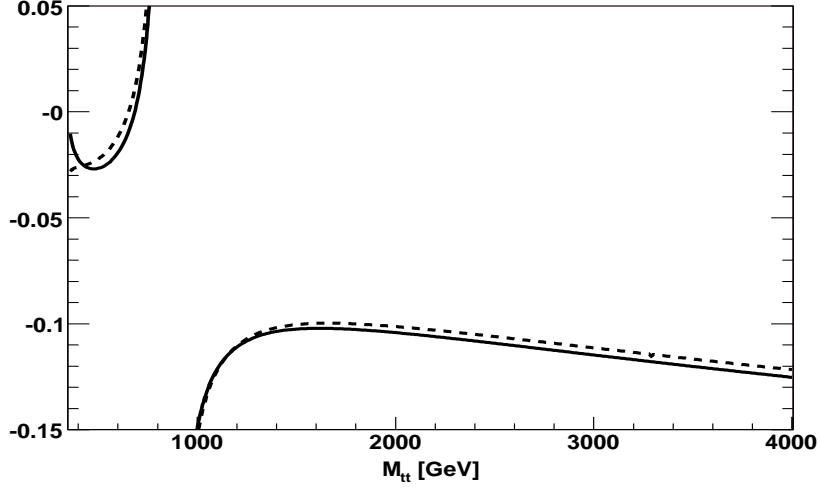


Figure 22: The ratio  $A_{hel}^{weak}/A_{hel}^{LO}$  of the contributions to the double spin asymmetry  $A_{hel}$  for the LHC ( $gg$  subprocess only). The solid and dotted line corresponds to  $m_H = 120$  GeV and  $m_H = 200$  GeV, respectively.

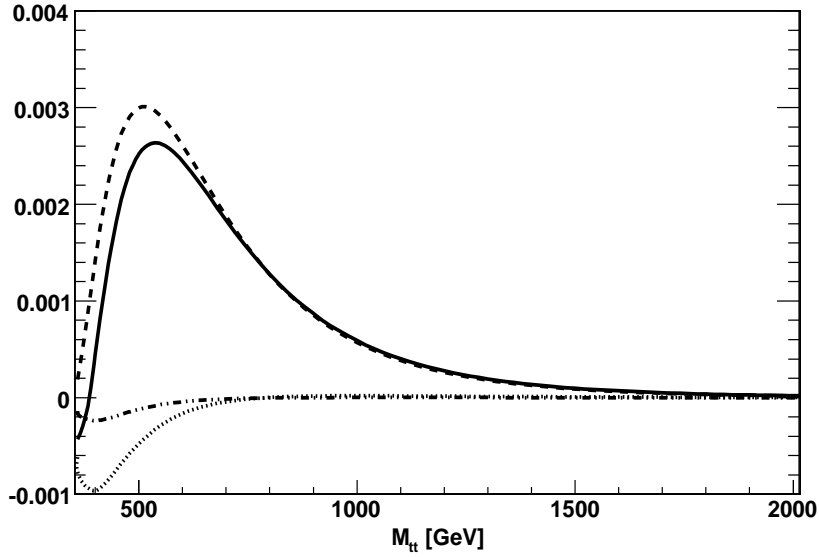


Figure 23: The P-violating differential spin asymmetry  $Z_{hel}$ , defined in (3.6), in units of [pb/GeV] at the LHC. Contribution from the  $gg$  (dashed line) and  $q\bar{q}$  (dotted line) subprocesses, and their sum (solid line). The dash-dotted line is the contribution from the  $qg$  and  $\bar{q}g$  subprocesses.

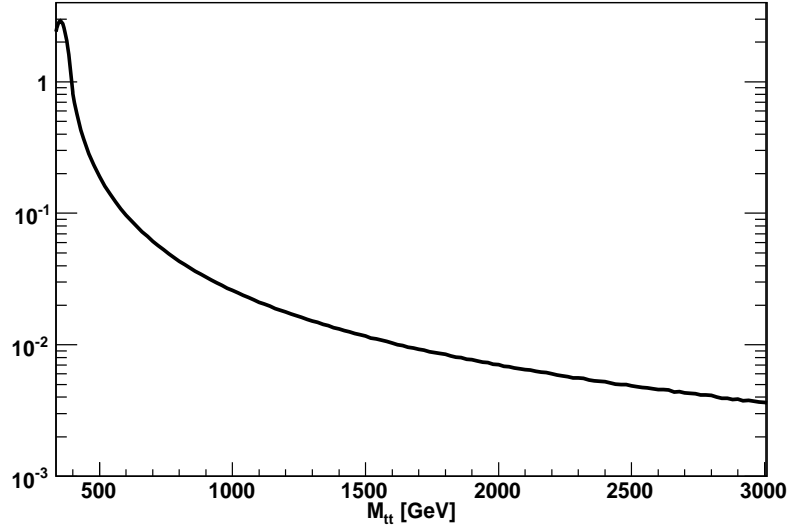


Figure 24: The ratio  $(-1)(Z_{hel} + \bar{Z}_{hel})/(Z_{hel} - \bar{Z}_{hel})$ , where  $Z_{hel}$  and  $\bar{Z}_{hel}$  are defined in (3.6), at the LHC.

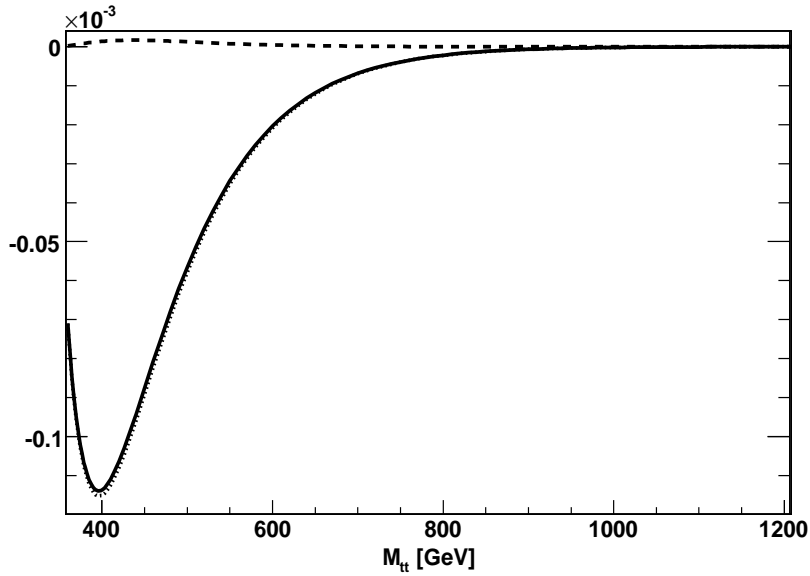


Figure 25: The P-violating differential spin asymmetries  $Z_{RL} = Z_{hel}$ , defined in (3.5), (3.6), in units of [pb/GeV] at the Tevatron. Contribution from the  $gg$  (dashed line) and  $q\bar{q}$  (dotted line) subprocesses, and their sum (solid line).

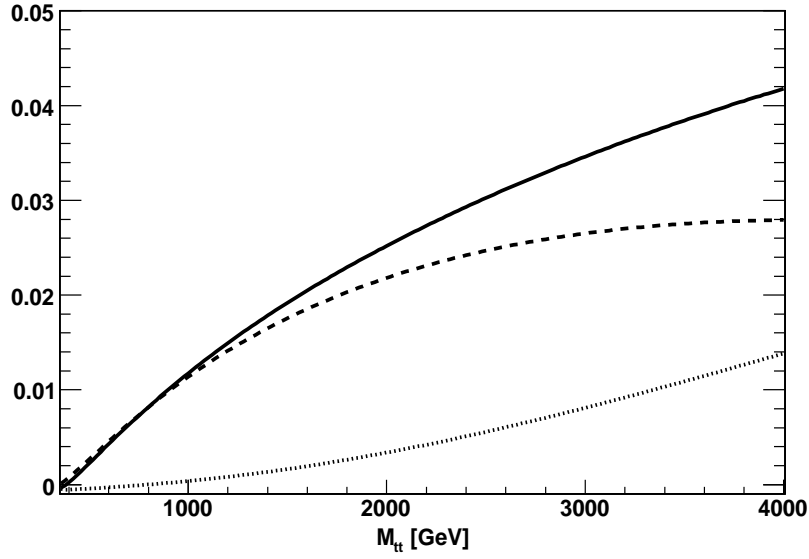


Figure 26: The P-violating differential spin asymmetry  $\Delta_{hel}$ , defined in (3.7), at the LHC. The dashed and the dotted line is the contribution from the  $gg$  and  $q\bar{q}$  subprocesses, respectively, and the solid line is the sum of both terms.

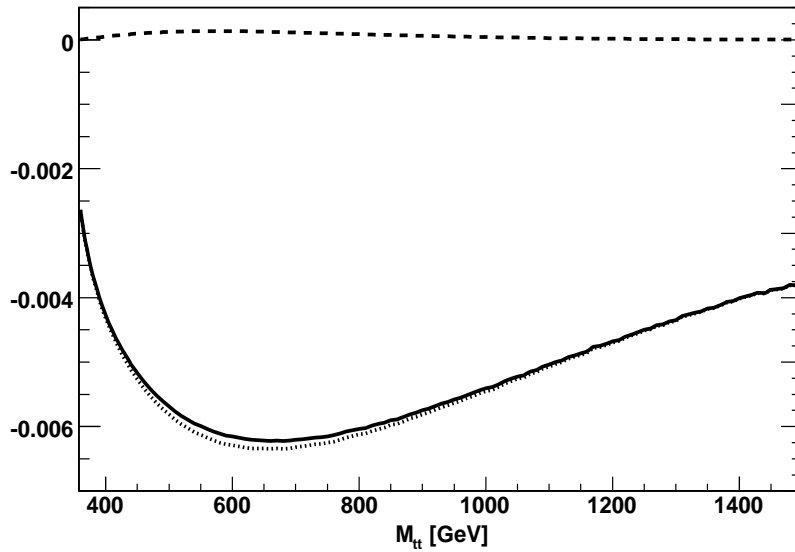


Figure 27: The P-violating differential spin asymmetries  $\Delta_{RL} = \Delta_{hel}$ , defined in (3.5), (3.7), at the Tevatron. The dashed and the dotted line is the contribution from the  $gg$  and  $q\bar{q}$  subprocesses, respectively, and the solid line is the sum of both terms.